AD NUMBER

AD272653

NEW LIMITATION CHANGE

TO

Approved for public release, distribution unlimited

FROM

No Foreign

AUTHORITY

DTRA Ltr., 6 May 99

WATERWAYS EXPERIMENT STATION
CORPS OF ENGINEERS, UNITED STATES ARMY
CONTRACT DA-22-079-ENG-224
R & D SUBPROJECT 8-12-95-420
AND THE DEFENSE ATOMIC SUPPORT AGENCY
NWER SUBTASK NO. 13.009

THE RESPONSE OF SOILS
TO DYNAMIC LOADS

REPORT 6

EFFECTS OF RATE OF STRAIN ON STRESS-STRAIN BEHAVIOR OF SATURATED SOILS

ARCHIE M. RICHARDSON, JR.

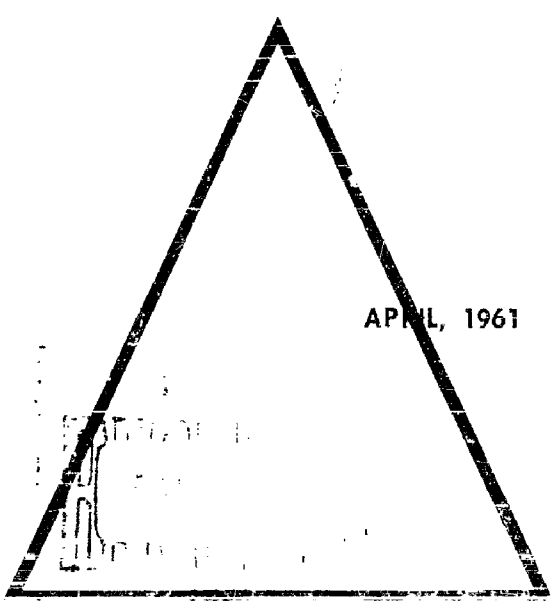

MASSACHUSETTS INSTITUTE
OF TECHNOLOGY

DEPARTMENT OF CIVIL
AND SANITARY ENGINEERING
SOIL ENGINEERING DIVISION
PUBLICATION 110

APRIL, 1961

ERRATA

THE RESPONSE OF SOILS TO DYNAMIC LOADS;
REPORT 6, EFFECTS OF RATE OF STRAIN ON STRESS-STRAIN
BEHAVIOR OF SATURATED SOILS

April 1961

This Errata Sheet supersedes in its entirety the previous Errata Sheet distributed in February 1962. Please make changes indicated on attached Errata Sheet to your copy/copies of DASA-1237 published by the Massachusetts Institute of Technology for the U. S. Army Engineer Waterways Experiment Station and the Defense Atomic Support Agency under Contract No. DA-22-079-ENG-224, R&D Subproject 8-12-95-420.

ERRATA SHEET

Page 4 line 7: Replace Table 2.1 with Table 2.2

Page 6 line 6: Replace ϕ'_e with ϕ_e

Page 8 Add the following column to the right of Water Content at Failure

"As-trimmed" Water Content

--
--
--
32.5
29.3
32.3
--
32.4
29.3
--
--
31.8
32.6
31.2
--
31.5
32.8
--

Page 10 line 14: Delete period after "2.16" and insert for Tests 1, 2, 3, and 4.

Section 2.5 heading: Replace - During Tests with - Drained Tests

Page 11 line 12: Delete entire first sentence of paragraph

Page 14 line 4 under Section 2.7: Replace main series with preliminary series

Page 16 line 3: Replace Figure 2.14 with Figure 2.17

line 14: Replace sin ϕ with sin ϕ'

Page 18 line 4: Replace Figure 2.8 with Figure 2.18

Page 21 lines 11-12 under Section 2.10: Replace Figure 2.2 with Figure 2.21

Page 21 line 13 under Section 2.10: Replace Tests P-2 and P-3 with Tests P-2 and 3

last word on page: Replace interaction with intersection

Page 67 Figure 3.2: Replace Stress (kg/cm^2) on vertical axis with Stress (lb/in^2) and Consolidation Pressure = 4 kg/cm^2 with Consolidation Pressure = 56.8 lb/in^2

Page 68 Figure 3.3: Replace Consolidation Pressure = 4 kg/cm^2 with Consolidation Pressure = 56.8 lb/in^2 and Total Lateral Pressure (σ_3) = 4 kg/cm with Total Lateral Pressure (σ_3) = 56.8 lb/in^2

THE RESPONSE OF SOILS TO DYNAMIC LOADINGS

Report 6: EFFECTS OF RATE OF STRAIN ON STRESS-STRAIN BEHAVIOR OF SATURATED SOILS

Archie M. Richardson

April, 1961

Soil Engineering Division
Massachusetts Institute of Technology
for
U.S. Army Engineers, Waterways Experiment Station
Department of the Army
R and D Subproject 8-12-95-420
Contract No. Da-22-079-eng-224
and for the
Defense Atomic Support Agency
NWER Subtask No. 13.009
Requests for copies of this report should be submitted to
ASTIA, Arlington Hall Station, Arlington 12, Virginia

LIST OF CHAPTERS

TABLE OF CONTENTS

LIST OF FIGURES

LIST OF TABLES

DISTRIBUTION LIST FOR DASA-1237

Addressees	No. of Copies
Bureau of Mines, Washington, D. C. ATTN: J. E. Crawford	1
Chief, Bureau of Yards and Docks, ND, Washington 25, D.C. ATTN: D-440	1
Chief, Defense Atomic Support Agency, Washington 25, D.C. ATTN: Document Library ATTN: Major Vickery	12 1
Chief of Engineers, Department of the Army, Washington 25, D.C. ATTN: ENGRD-S ATTN: ENGMC-EB	3 2
Chief of Naval Operations, ND, Washington 25, D. C. ATTN: Op-75	1
Chief of Research and Development, DA, Washington 25, D.C. ATTN: Atomic Division	1
Commander, Air Force Ballistic Missile Division, Air Research and Development Command, ATTN: WDFN P. O. Box 262, Inglewood 49, Calif.	1
Commander, Armed Services Technical Information Agency (ASTIA), Arlington Hall Station, Arlington 12, Va.	20
Commander, Air Force Special Weapons Center, Kirtland Air Force Base, Albuquerque, N. M., ATTN: SWRS	4
Commander, Wright Air Development Center, Wright-Patterson Air Force Base, Ohio, ATTN: WCOSI	1
Commanding Officer and Director, U. S. Naval Civil Engineering Laboratory, Port Hueneme, Calif.	1
Director, Weapons Systems Evaluation Group, OSD, Room 1E880, The Pentagon, Washington 25, D. C.	1
Director, U. S. Army Engineer Waterways Experiment Station, P. O. Box 631, Vicksburg, Miss.	20

Addressees	No. of Copies
Director of Civil Engineering, Headquarters, U. S. Air Force, Washington 25, D. C., ATTN: AFOCE	1
Director of Defense Research and Engineering, Washington 25, D.C. ATTN: Technical Library	1
Headquarters, U. S. Air Force, Washington 25, D. C. ATTN: AFTAC, C. F. Romney	2
U. S. Coast and Geodetic Survey, Washington, D. C. ATTN: D. S. Carder	1
U. S. Coast and Geodetic Survey, San Francisco, Calif. ATTN; W. K. Cloud	1
U. S. Geological Survey, Washington, D. C. ATTN: J. R. Balsley	1
American Machine and Foundry, 7501 North Natchez Avenue Niles 48, Illinois, ATTN: Mr. Tom Morrison	1
Dr. Harold Brode, RAND Corporation, 1700 Main Street, Santa Monica, California	1
California Institute of Technology, Pasadena, Calif. ATTN: F. Press ATTN: H. Benioff	1 1
Columbia University, New York, N.Y., ATTN: J. E. Oliver	1
Barry Wright Corporation, 700 Pleasant Street, Watertown 72, Mass., ATTN: Mr. Cavanaugh	1
Edgerton, Germeshausen, and Grier, Inc., Los Vegas, N.M. ATTN: H. E. Grier	1
Holmes and Narver, Los Angeles, Calif., ATTN: S. B. Smith	1
Mr. Kenneth Kaplan, Broadview Research Corporation, 1811 Trousdale Drive, Burlingame, Calif.	1
Professor Robert L. Kondner, The Technological Institute, Northwestern University, Evanston, Ill.	1
Professor Gerald A. Leonards, School of Civil Engineering, Purdue University, Lafayette, Indiana	1

Addressees	No. of Copies
Atomic Defense Engineering Department, Pennsylvania State College, State College, Pa., ATTN: Professor Albright	1
Dr. N. M. Newmark, Civil Engineering Hall, University of Illinois, Urbana, Ill.	1
Mr. W. R. Perret, 5112, Sandia Corporation, Sandia Base, Albuquerque, N. M.	1
Professor F. E. Richart, Jr., Department of Civil Engineering, University of Florida, Gainesville, Fla.	1
Mr. Fred Sauer, Physics Department, Stanford Research Institute, Menlo Park, Calif.	1
Dr. T. H. Schiffman, Armour Research Foundation, Illinois Institute of Technology, Technology Center, Chicago 16, Ill.	1
Professor H. Bolton Seed, Department of Civil Engineering, University of California, Berkeley, Calif.	1
Space Technology Laboratory, Inglewood, Calif., ATTN: B. Gussholz	1
Stanford Research Institute, Physical Sciences Division, Menlo Park, California., ATTN: Dr. R. B. Vaile, Jr.	2
Mr. A. A. Thompson,, Terminal Ballistics Labooratory, Aberdeen Proving Ground, Aberdeen, Md.	1
Professor J. Neils Thompson, Civil Engineering Department, University of Texas, Austin 12, Tex.	1

Chapter 1

INTRODUCTION

1.1 Background

The research described in the following report was performed under Contract No. DA-22-079-eng-224 between the Waterways Experiment Station, a research facility of the Corps of Engineers, United States Army, and the Massachusetts Institute of Technology. The work has been sponsored by: (1) the Army Research and Development Program for Nuclear Weapons' Effects on Structures, Terrains, and Waterways, Subproject 8-12-95-420; (2) the Army Research and Development Program for Ground Mobility Research, Subproject 70-05-400; and (3) the Defense Atomic Support Agency, a joint agency of the three armed services.

The previous research under this contract is described in (MIT 1959b). The overall objective of this research is very adequately described in that report. However, in summary, the ultimate aim of this research is an understanding, at the fundamental level, of the nature of the patterns of behavior of soil media subjected to rapidly applied loads and of the mechanisms leading to these behavior patterns.

1.2 Scope of research

The scope of the research under this contract is the same as described in (MIT 1959). In this study of the behavior of soils under rapidly applied loads, three approaches have been employed: (a) Research into the behavior of soils under rapidly applied loads in triaxial compression; (b) Research into the behavior of soils under rapidly applied loads in one-dimensional compression; and (c) a study of wave propagation in soil media.

In research studies of the behavior of soils in one-dimensional and triaxial compression, a dead-end was rapidly reached since only the total applied stresses were known. It has thus become necessary to extend this

research by introducing a program which involved the development and use of devices for measurement of the pressure induced in the water occupying the interparticle voids in the soil media at the encountered stress levels and times of loading.

The work completed under this research effort during the period October 1959 to October 1960 has been or is being reported in three separate reports as follows: (a) a report on the development and performance of devices for rapidly measuring pore-water pressure; (b) this report on triaxial compression research; and (c) a report covering the work accomplished under the one-dimensional compression and wave propagation aspects of the research.

1.3 Triaxial compression research

The triaxial compression research performed in the past under this contract and described in (MIT 1959b) has been conducted mainly on compacted soil specimens. This research, while yielding much useful information regarding the effects of the rate of strain on the stress vs. strain behavior of soil media could not be expected to yield much information concerning the mechanisms of the observed behavior since one vital piece of information was missing. Unless the results of research of this type can be analysed in terms of effective stresses, (total stresses minus the hydrostatic pressure in the fluid phase) little knowledge can be gleaned regarding the mechanism which allows soils to resist shear stress or the manner in which the rate of stress application affects this mechanism.

During the past contract period (October 1959 to October 1960) considerable effort has been expended in the development of a device allowing rapid measurement of the pressure in the fluid phase of the soil media. This work has met with considerable success and devices are now being used which permit very rapid measurement of this pore water pressure. The state of development of these devices as of October 1960 is described in a companion report. As non-saturated soil media are three phase systems in which soil skeleton, fluid

and gas interact in a complicated manner to give the system its external behavior characteristics, the best initial approach would seem to be through saturated systems in which no free gas is present. Soil engineers are now in general beginning to describe and explain effectively, in terms of effective stresses, the behavior of saturated soils; thus, it was decided that a comprehensive investigation into the effect of rate of strain on the manner in which saturated soils resist shear stresses should be undertaken.

1.4 Scope of this report

This report contains descriptions and results of research into the effect of rate of strain on the shear stress resistance of saturated fine-grained soils. The following portion of this report contains three parts: (1) description of static triaxial compression tests on a Loess (representative of a lean clay); (2) description of rapid triaxial compression tests on this same soil; and (3) a description of rapid triaxial tests on a fat clay. It is, of course, necessary to completely describe in a consistent manner the patterns of behavior of the two soils during static or very slowly applied stresses before the relationship of the changes in these behavior patterns to rate of strain can be determined. Thus "static" triaxial tests form a very important part of research into the response of soils to "dynamic" loads.

1.5 Acknowledgements

The research work reported herein has been performed by the Soil Engineering Division of the Civil and Sanitary Engineering Department. Professor T. William Lambe, as head of the Soil Engineering Division has overall responsibility for the work. Professor Robert V. Whitman has immediate responsibility for this work. This report has been prepared by Archie M. Richardson, Jr. who, together with Nasim M. Nasim, carried out the research. Both were Research Assistants during the period covered by this report.

Chapter 2

STATIC TRIAXIAL COMPRESSION TESTS ON SATURATED LOESS

2.1 Introduction

This chapter presents the results of a series of triaxial compression tests on samples of saturated loess consolidated from a slurry. A total of eighteen tests were carried out. Sixteen consolidated, undrained tests with pore pressure measurements were performed. Three of these were of a preliminary nature performed on molded specimens saturated by backpressuring. Two tests were consolidated, drained tests. The results of these tests are summarized in Table 2.1, and detailed results are presented in the various figures accompanying this chapter.

2.2 Properties of soil

The soil used in this series of tests was a loess, typical of deposits of the lower Mississippi River Valley. A 55 gallon drum of this soil was received from the Waterways Experiment Station in December, 1958. The soil classifies as an ML soil according to the Unified Classification System and exhibits a Liquid Limit of 37% (34% to 40%) and a Plasticity Index of 11% (8% to 14%). As is typical of windblown deposits, the grain size is rather uniform, 72% of the particles falling within the silt size range. 4% of the particles are sand size ($>$ 0.06 mm.) and 14% are clay size ($<$ 2 microns). The clay fraction is illite-montmorillonoid clay while the silt sized particles are largely quartz. A complete mineralogical analysis of this soil along with other pertinent data appears in (MIT 1959b).

2.3 Preparation of samples

The main series of fifteen consolidated drained and undrained tests was performed using test specimens trimmed from a large cylinder of the soil which had been consolidated from a slurry. The three preliminary tests were performed upon specimens formed by pressing soil of a consistency lower than

the liquid limit but well wet of Proctor optimum, into a Teflon cylinder $1\frac{1}{2}$ inches in inside diameter. Specimens of the appropriate size were subsequently trimmed from the cylinders extruded from this Teflon mold. Of course, the specimens formed in this manner could not be expected to be saturated. Consequently, an attempt was made to saturate them following triaxial consolidation by raising both the total all around pressure (chamber pressure) and the pore water pressure by the same amount and thus diminish the size of any air bubbles by driving air into solution and reducing the volume of any remaining air (according to Henry's and Boyle's laws, respectively).

Specimens for the main series of test were prepared by consolidation from a slurry in the following manner. A quantity of soil was removed from the drum, broken into small lumps and air-dried. The air-dried soil was passed through a mechanical grinder. This grinder is capable of grinding a soil, such as the Loess, until all particles will pass a No. 100 sieve.

The ground Loess was thoroughly mixed with deaired, demineralized water to a consistency well above the liquid limit, and this slurry was left to temper for 24 hours. Following tempering, the slurry was extruded or atomized into an evacuated large consolidometer. A sketch of this large consolidometer appears in Figure 2.1 while a schematic sketch of the method of introducing the slurry is shown in Figure 2.2. Following the introduction of the slurry, the top portion of the consolidometer was replaced and the soil was consolidated. The load was applied in five increments, each double the previous, the final increment being 1 kg./cm.^{2}, i.e., 1/16, 1/8, 1/4, 1/2, and 1 kg./cm.^{2}. Each increment was allowed to remain until 100% primary consolidation was complete, about 3 days. The final load of 1 kg./cm.^{2} was permitted to remain on the sample for one week.

Following consolidation, the soil cake ($9\frac{1}{2}$ inches in diameter by $5\frac{1}{2}$ inches high) was extruded and cut into 15 rectangular prisms. The water content of the soil at this time averaged 32.4%. The individual prisms were stored by immersing them in a very inert, water repellent oil in an aquarium

TABLE 2.1

ENGINEERING PROPERTIES - SATURATED LOESS

1. Normally Consolidated

   $c' = 0$

   $\varphi' = 26\ 1/2^{\circ}$

2. $C_c = 0.18$

3. $C_r = 0.04$

4. $\varphi'_e = 13^{\circ}$

5. $\mathcal{H} = \frac{c_e}{p_e} = 0.13$

tank. (Mobil No. BB Transformer oil was used). Table 2.2 contains a tabulation of the water contents of samples trimmed from these oil-stored prisms, and it will be seen that with the exception of samples 2 and 6, there is little indication of any water content change occurring during storage.

The preceding method of preparing deaired, saturated samples of remolded soil has met with considerable success when used to prepare samples of fat clay. Approximately one dozen batches of the Fat Clay (MIT 1959b) have been prepared in this manner along with several batches of minus 2 micron kaolinite. With few exceptions, excellent results were obtained, there being very little reason to doubt that the vast majority of samples thus obtained have a degree of saturation of 100% and that the exceptions were still very highly saturated, approaching 100%. However, difficulty was experienced in preparing saturated samples of the Loess. When Loess was mixed and atomized into the consolidometer at a water content wet enough to assure complete removal of air bubbles during the atomization process, segregation of grain sizes was observed in the slurry following its deposition when the silt size particles settled and the clay size particles remained in a thin layer at the upper portion of the slurry.

Since the 14% clay portion of the Loess exerts a major influence on its stress-deformation behavior, any loss or irregular distribution of fines seriously affects the resulting behavior of the soil. As an example, the first batch was quite wet when placed, and the subsequent behavior was so erratic as to warrant disposing of this batch (e.g., some of the samples actually dilated during shear stress application as would be expected with a dense silt, rather than decreasing in volume as is typical of a normally consolidated lean clay. Conversely, if the soil were to be placed in the consolidometer at a water content low enough to preserve the original grain size distribution, high degrees of saturation could not be obtained.

The final soil samples represent a condition midway between these extremes. Consequently, the final samples exhibited marked non-uniformities along with incomplete saturation. The erratic water content versus logarithm

TABLE 2.2

DATA FROM STATIC TRIAXIAL COMPRESSION TESTS - SATURATED LOESS

Test No.	Maximum Consolidation Pressure (kg/cm^2)	σ_3 prior to testing	Overconsolidation Ratio (OCR)	Water Content at Failure (%)	$\frac{(\sigma_r - \sigma_3)}{2}$ max. (kg/cm^2)	Equivalent at Failure (kg/cm^2)	Pore Pressure Response Prior to Backpressuring - %		Backpressure (kg/cm^2)
							1 min.	10 min.	
P1	8.0	1.0	8	22.3	1.19	0	—	30	1.0
P2	4.0	4.0	N.C.	21.2	1.55	2.5	—	30	2.0
P3	2.0	2.0	N.C.	23.6	.57	1.4	—	30	2.0
1	8.0	8.0	N.C.	24.4	2.29	4.6	30	30	0.9
2	4.0	4.0	N.C.	24.8	1.40	2.4	66	95	3.9
3	2.0	2.0	N.C.	28.0	.57	1.08	80	95	2.2
4	1.0	1.0	N.C.	29.4	.44	.30	85	95	1.95
5	8.0	4.0	2	25.4	2.27	2.2	68	68	2.0
6	8.0	1.0	8	26.6	1.22	-0.4	75	75	2.24
7	8.0	2.0	4	25.6	1.57	+0.6	85	85	3.0
8	8.0	0.5	16	26.6	1.16	-0.65	64	80	1.5
9	8.0	0.25	32	27.5	.93	-0.50	83	93	0.75
10	8.0	4.0	2	25.7	1.67	2.42	80	87	3.0
11	3.0	3.0	N.C.	24.3	2.29	0			0
12	5.0	5.0	N.C.	23.7	3.84	0			0
13	2.0	2.0	N.C.	29.5	.55	1.53	85	98	2.0
14	4.0	4.0	N.C.	27.7	1.05	2.50	84	96	2.0
15	8.0	8.0	N.C.	25.4	2.32	5.42	38	38	1.0

of applied pressure data (Figure 2.16) and slightly nonconsistent behavior during application of shearing stresses illustrates both of these conditions, while the less than 100% pore pressure response is indicative of a degree of saturation less than 100% (See Table 2.2) This problem of obtaining uniform, saturated samples represents one of the drawbacks to utilizing this particular soil type in any extensive research investigation.

2.4 Triaxial consolidation

Individual specimens for triaxial testing were trimmed either from the soil extruded from the Teflon mold or from the soil prisms stored in oil. A standard size of specimen 1.40 inches in diameter by 3.15 inches in height was chosen. Each specimen was placed upon a porous stone on the pedestal of a triaxial cell of Norwegian Geotechnical Institute design and manufacture (NGI 1957). Six strips of filter paper, 3/16 inch in width, were affixed to each specimen at equal spacings and extended vertically from the top of the specimen down to and overlapping the circumference of the porous stone. The drainage lines from the pedestal of the cell base, the porous stone and the filter paper strips had previously been filled or saturated with thoroughly deaired water. A solid lucite top cap was placed atop each specimen, and each specimen was encased in two thin latex membranes separated by a layer of silicone grease of the type used to grease stopcocks. The membranes were sealed to the lucite top cap and to the triaxial cell pedestal by four "O" rings, two on top and two on the bottom.

The triaxial cell cylinder was fastened to the base and filled with deaired water. A burette was affixed to the drainage line to measure drainage, and pressure was supplied to the chamber by the standard NGI constant pressure cell (NGI 1957). In the sixteen tests which were to be run undrained, the drainage line was blocked following consolidation and backpressuring. Therefore, as the water content could not change following the closing off of drainage, the water content obtained at the end of shear testing was that existing at equilibrium under the effective stress system at 100% primary consolidation.

The results of triaxial consolidation are plotted in the usual water content versus logarithm of effective consolidation pressure plot in Figure 2.16. It is apparent from this plot that considerable scatter of data occurs. An extreme anomaly occurs between the water contents obtained in the preliminary tests and those obtained in the main series. The most important factor contributing to this scatter is probably the lack of saturation of the samples. Much weight is added to this opinion by the following two observations: (a) the slope of both the normal consolidation and rebound lines drawn for the preliminary series of tests almost exactly parallels the slope of the corresponding line for the main series of tests, and (b) the plots of the stress paths (Figure 2.17) exhibit behavior indicative of a higher isotropic consolidation pressure. Corrected points, based on these stress paths, have also been plotted in Figure 2.16. For these reasons, considerable weight has been given those points exhibiting the highest water contents for any effective consolidation pressure in drawing the normal consolidation and rebound lines.

Assuming a specific gravity of solids, $G_s = 2.76$, the Compression Index, $C_c = 0.179$, and the Rebound Index, $C_r = 0.037$, can be obtained from the data plotted in Figure 2.16. It is also interesting to note the close agreement with the normal consolidation lines of the point representing the average "as trimmed" water content plotted against the vertical consolidation pressure in the large consolidometer.

2.5 Triaxial Compression Testing - During Tests

Drained triaxial compression tests were performed on two samples, both normally consolidated, in Tests 11 and 12. In these tests, following consolidation, deformation of the test specimen proceeded at a rate of axial strain slow enough to allow complete dissipation of excess pore water pressures. Thus the hydrostatic pressure existing in the triaxial chamber was the same as the effective minor principal stress acting on the sample. There are two drawbacks to this type of test:

(a) The length of time required for the test is, in most cases, excessive, and (b) excessive sample deformation is required to reach the maximum deviator stress, and as a result, both piston friction and the validity of the usual area corrections give cause for grave concern. However, these drawbacks are often offset by the relative ease of performance of this type of test which often leads to less ambiguous results than those obtained in other types of tests. As will subsequently be discussed, recently advanced theories (HENKEL, 1959) have led to a greater usefulness of this type of triaxial test in allowing prediction of pore pressures and stress paths in undrained tests from the results of drained triaxial tests.

Table 2.3 is a tabulation of the rates of strain used in the performance of the drained tests. Assuming failure at 6% strain in Test 11 and 10% in Test 12, times to failure of 36.5 hours and 41 hours, respectively, were required. BISHOP and HENKEL (1957), as a result of experience in testing clays, indicate a time to failure of 30 hours as a guide for a typical lean clay (Weald Clay, Liquid Limit = 43%, Plastic Limit = 18%). On this basis, the rates of strain used in Tests 11 and 12 seem more than adequately slow to insure complete drainage.

The stress versus strain volume change data from Test 11 are plotted in Figure 2.11 and for Test 12 in Figure 2.12. Some evidence of the trouble encountered from piston friction is shown in Figure 2.11. The points so indicated were obtained prior to a gentle rotation of the piston. Following this rotation, the loads as read on the proving ring dropped to values in keeping with the indicated curve. Following a leveling off of deviator stress almost no further trouble was experienced with piston friction.

In Test 12, the sample was strained to approximately 3% and the load frame was switched off overnight (approximately 15 hours). During this time the sample continued to strain approximately 1/2% with a resulting reduction in deviator stress. Following resumption of test-

TABLE 2.3

DATA FOR HVORSLEV PARAMETER PLOT - LOESS

Test	$\frac{\sigma_1 - \sigma_3}{2}$ (Fig. 2.20)	$\bar{\sigma}_3$ Failure	p_e	$\frac{\sigma_1 - \sigma_3}{2p_e}$	$\frac{\bar{\sigma}_3}{p_e}$
P-1	1.15	1.0	5.50	.209	.182
P-2	1.55	1.73	4.00	.388	.433
P-3	.57	1.05	2.00	.285	.525
1	2.29	3.41	8.00	.286	.426
2	1.40	2.25	4.00	.350	.563
3	.57	1.45	2.00	.285	.725
4	.44	.86	1.00	.44	.86
5	2.27	2.69	7.08	.321	.380
6	1.22	1.42	5.50	.222	.258
7	1.57	1.40	6.10	.257	.229
8	1.16	1.17	4.73	.245	.247
9	.93	.77	4.02	.231	.191
10	1.67	2.22	7.08	.236	.314
11	2.29	3.00	10.95	.209	.274
12	3.84	5.00	13.50	.284	.370
13	.55	.89	2.00	.275	.445
14	1.05	1.54	4.00	.263	.385
15	2.32	3.16	8.00	.290	.395

ing, the deviator stress rose sharply at a more or less constant strain, straining gradually began, and the resulting stress versus strain curve became apparently a continuation of the curve prior to "relaxation".

The areas used in computing the stresses were computed in the conventional manner considering both the volume change of the sample as recorded by the burette reading and the axial strain of the sample.

2.6 Triaxial Compression Testing - Undrained Tests

Sixteen specimens were tested in undrained triaxial compression following consolidation. In all of these tests, drainage from the sample was closed off at the completion of the consolidation process and connection was made to an appropriate device for measuring the pore water pressure. In the preliminary series of tests, connection was made to a null balance type of pore pressure measuring system of Norwegian Geotechnical Institute design (NGI 1957). In the main series of 13 tests, an automatic pore pressure measuring device was employed (PENMAN 1953). In this device, a sensing element detects any tendency toward migration of water from or toward the test specimen. The output of this sensing element controls a heater in a closed oil system. The expansion and contraction of this oil prevents the migration of pore water and operates a Bourden gauge indicating the pressure necessary to accomplish this, i.e., the pore water pressure.

In all samples, the first step following connection of the pore pressure measuring device was to increase rapidly the triaxial chamber pressure and, at the same time, note the resulting increase in pore water pressure, or pore pressure response. This response is a good indication of the degree of saturation of the entire system (soil sample, stone drainage connections and measuring device). If the system is completely saturated, the response of the pressure in the pore water should be immediate and equal to the increment of chamber pressure. As will be noted in Table 2.2, the response was poor in all cases. Since considerable care was exercised in assuring that the drainage connec-

tions and pore pressure measuring device were completely saturated, the most obvious source of the lack of good pore pressure response was the less than 100% saturation of the samples themselves. In order to offset the effects of this poor pore pressure response, two steps were taken: (1) the samples were backpressured as previously described, and (2) the tests were run as constant volume tests by maintaining constant pore pressures and adjusting the chamber pressures in such a manner that no flow of water either to or from the samples occurred. Since $\bar{\sigma} = \sigma - \mu$, a change in σ with a constant μ is equivalent to a corresponding change in μ with a constant σ.

The stress versus strain and pore pressure obtained from these tests are plotted in Figures 2.3 through 2.10 and 2.13 and through 2.15. In the main series of tests, the $\Delta\sigma_3$, necessary to maintain a constant volume, is plotted as an equivalent change in pore pressure. In the preliminary series, $\Delta\sigma_3$ is plotted directly.

Two rates of strain were used for the main series of tests. Tests 1 through 4 were performed at a rate of strain of 10% in 6 hours and the remainder were performed at a rate of 10% in 12 hours. The data give no evidence of any strain rate effect within the range.

2.7 Results of Triaxial Compression Tests on Loess

Engineering parameters of behavior of the Loess are presented in Table 2.1. All shear strength and pore pressure data are listed in Table 2.2. Figure 2.3 is a plot of the stress versus strain curves obtained from the main series of tests. The water contents obtained from the undrained series of tests are plotted against the logarithm of consolidation pressure in Figure 2.16.

2.8 Analysis of the Results of Triaxial Compression Tests on Loess

One of the most informative ways of analyzing the results of undrained triaxial tests is to plot the paths followed by the normal effective stress and shearing stress on some particular plane as the

test progresses to failure. Three planes are commonly selected for this purpose: (1) the plane of maximum obliquity of stresses; (2) the plane on which failure will ultimately occur, and (3) a plane at 45° to the principal stress planes. (This is the plane of maximum shear stress). The last two planes are the most informative and the stresses on these two planes are very closely related. The results of the normally consolidated tests are plotted thus in Figure 2.17 while the results of the overconsolidated tests are plotted in Figure 2.20.

In a plot of this type, the stress paths followed in a conventional drained test follow a path that starts at the particular value of the chamber pressure and progresses to failure on a straight line path inclined at 45° to the horizontal. These paths for Tests 11 and 12 are shown as dashed lines in Figure 2.17. A line connecting the points representing failure stress conditions for these two tests, and presumably for any other drained test on normally consolidated samples is shown and is labeled the CD (Consolidated-Drained) line. It is interesting to note that this line, with minor exception, fails through points of maximum deviator stress (but not points of maximum stress obliquity) on the stress paths for undrained tests.

Apparently the specimens tested in Tests 13, 14 and 15 were the most fully saturated as they gave the maximum water contents when plotted in Figure 2.16 and the stress paths from these three tests are extremely typical of stress paths from undrained tests on saturated clay soils. Tests 1, 2, 3 and 4 present atypical stress paths. Rather than commencing with a tangent having a negative slope or a slope of infinity (both are typical), the stress paths from these tests commence with tangents having a positive slope. This behavior is typical of heavily overconsolidated soils or of soils tested in situations where drainage was known to occur. The most probable explanation of the stress path from these tests lies in the lag in the pore pressure measuring systems. Due to these lags, the volume of the specimens decreased (as in a drained test) prior to the detection of this tendency by the test operator. As the test progresses,

the stress paths merged with a hypothetical stress path from a test normally consolidated to higher pressure. The dotted curve extension to the stress path of Test 2 in Figure 2.14 represents an approximation to such a hypothetical curve. An assumption that the failure water content of Test 2 is that attained by a consolidation pressure of $4.75\ kg/cm^2$ would move the point representing Test 2 to the right as shown in Figure 2.16. This has also been indicated in Figure 2.16 for Tests 1, 3 and 4.

The angle α giving the slope of the CD Line in Figure 2.17 is related to the usual ϕ' or drained angle of shearing resistance obtained from a plot of shear stress on the failure plane at the time of failure plotted against the stress normal to the failure plane at the time of failure by the relationship:

$$\sin\varphi = \tan\alpha = 0.438;\ \varphi' = 26^{\circ}.$$

Stress paths from the overconsolidated tests have been plotted in Figure 2.20 in a manner similar to the normally consolidated tests. Tabulated in this figure is the overconsolidation ratio (OCR) pertaining to each particular test. This value is the ratio of the maximum past pressure to the effective stress existing on the sample prior to testing (i.e., $OCR = \frac{\bar{\sigma}\ \text{cons max.}}{\bar{\sigma}\ \text{rebound}}$). A stress vector representing an average of Tests 1 and 15 has been plotted to complete this plot with a stress path representing an OCR = 1 (or normal consolidation). These stress paths are reasonably typical and a rather well defined "failure envelope" can be drawn, as shown. However, the following anomalous behavior can be seen in a close study of Figure 2.20: (1) the stress paths of Tests 5 and 10 should coincide since the stress histories of these two samples prior to testing are identical. The fact that the two stress paths do not

coincide probably reflects a rather basic dissimilarity of composition between these two samples as the water contents are quite similar, and the difference in water content that does exist would tend to produce behavior differences opposite to that observed in Figure 2.20. (2) Stress paths from Tests 5 and 7 proceed to the assumed "failure envelope" in a typical manner and then exhibit a pronounced reversal of behavior, moving out into the domain past the failure envelope on a path of almost constant deviator stress (i.e., by an increase of pore water pressure).

The stress path of Test 10 exhibits a similar phenomenon in a somewhat different manner. The divergence from typical behavior occurs before the failure envelope is reached, and the stress path reaches and rides along the envelope in a somewhat atypical fashion. The explanation for this irregular behavior may be found in the interrelationship between the fraction of the soil particles that would behave as a granular media (i.e., the majority of the silt size) and the matrix of fines behaving colloidally (i.e., the clay fraction). The failure envelope as shown could then represent the stress behavior of the clayey matrix, and the anomalies occur when the skeleton of silt size particles begins to contribute to the behavior. The straight line approximation to the failure envelope for this case can be described by the parameters b = intercept on y axis = .32 kg/cm^2 and α = slope of failure envelope = Tan^{-1} .370 or converted to ϕ' = 21 1/2° and c' = 0.34 kg/cm^2.

2.9 Idealization of the behavior of Loess in triaxial compression

The preceding discussion points out the wide scatter of the data resulting from these triaxial compression tests. In this section an attempt will be made to idealize the behavior in such a manner that future studies of the effect of rate of strain on the stress vs. strain behavior may be compared to it.

Attention will be first directed to the normally consolidated tests. In Figure 2.17, each stress path from an undrained test represents a line of

constant water content. Tests 14 and 15 represent the typical behavior to be expected. These two curves were "normalized" by dividing both the ordinates and abscissas of points on the curve by the pressure to which the particular sample was consolidated. These normalized points were plotted in Figure 2.8, and a best fit curve rising to the consolidated-drained failure line was drawn. Using the plot of water content vs. logarithm of consolidation pressure, this normalized, idealized stress path was expanded to the family of curves in Figure 2.19. It has been proposed and data have been presented to support the proposal (HENKEL, 1959) that such water content contours are unique curves relating the pore pressures developed in undrained tests to the volume changes occurring in drained tests. Henkel's data are plotted in principal stress space to obtain as general a relationship as possible, but the hypothesis is equally valid for the simple type of plot shown here.

As each curve represents a constant water content, it represents the stress path followed in an undrained test consolidated to the pressure indicated. For example, a sample of remolded loess, consolidated to 4 kg/cm^2, should ideally have a water content of 27.3%. If subjected to an undrained triaxial compression test following consolidation, it should follow the effective stress path represented by the 27.3% water content contour, reaching the failure envelope at a deviator stress of 1.05 kg/cm^2. The total stress path during testing is represented by the dashed line 4-B. The pore pressure at any stage in the test is the horizontal distance between the total stress and the effective stress paths. At failure the pore pressure would be the horizontal distance AB or 2.60 kg/cm^2. The pore pressure parameter A equals

$$\frac{u}{\Delta(\sigma_1-\sigma_3)} = \frac{2.60}{2 \times 1.05} = 1.24$$

(SKEMPTON, 1954).

The dotted lines on Figure 2.19, starting at 3.0 kg/cm^2 and 5.0 kg/cm^2 on the x axis and rising with a slope of 45^o, represent stress paths of drained triaxial compression tests consolidated to these chamber pressures. If the water content contours are unique, the points where the stress paths cross water content curves should yield the water contents existing in the drained triaxial tests at these stress levels. Tests 11 and 12 are triaxial tests of

this nature. Assuming a water content prior to application of the deviator stress corresponding to Figure 2.19, and making use of the volume change data given in Figures 2.11 and 2.12, a comparison of predicted and actual water contents can be made. This comparison is made in Table 2.4. At first glance the calculated water contents in Test 11 seem to present rather poor agreement with the predicted values. However, closer inspection reveals the fact that discrepancy occurs between the start of the test and point 2, with the difference in calculated and predicted water contents remaining almost constant from point 2 to point 6 at maximum deviator stress. A study of Figure 2.19 leads to the conclusion that as the stress path reaches the failure envelope, if the deviator stress reaches a constant value, no further volume change should result with additional straining. However, in the actual test, a volume change was occurring as maximum deviator stress was reached and continued to occur up to the end of testing. If the volume change at the end of testing is used to compute the water content in Table 2.4, very close agreement with the predicted value occurs. A possible explanation for this occurs in a non-uniform distribution of stresses and hence a non-uniform distribution of water contents in such a test. This variation in water content could have begun to occur at the beginning of testing and reached an equilibrium distribution between stress levels represented by points 1 and 2. Following the attainment of a maximum deviator stress condition, this special distribution of water content began once more to equalize itself, becoming almost uniform at failure.

Test 12 presents calculated vs. predicted values in quite good agreement up to the stress level where relaxation was permitted. Following the resumption of testing, these values diverged somewhat at large strains. Considering the uncertainties involved in these types of measurements and prediction, quite good agreement between the predicted and calculated water contents seem to be attained.

No idealization of the overconsolidated tests has been made. It is felt that insufficient data is available to allow resolution of some of the anomalies apparent in Figure 2.20. However, if some average path representing Tests 5

TABLE 2.4

COMPARISON BETWEEN OBSERVED AND PREDICTED $\bar{\omega}$-DRAINED TESTS - SATURATED LOESS

Point	$\frac{(\sigma_1 - \sigma_3)}{2}$	ΔV (cc) (Fig. 2.11)	Volume of Water (cc)	Water Content (calculated) (%)	Water Content (predicted) (%)
			TEST 11		
3 kg/cm^2	0	0	33.5	28.1	28.1
1	.77	.27	33.23	27.9	27.3
2	1.26	.70	32.80	27.5	26.6
3	1.63	1.18	32.32	27.2	26.1
4	1.95	1.57	31.93	26.8	25.6
5	2.20	1.92	31.58	26.5	25.3
6	Max $(\sigma_1 - \sigma_3)$	2.0	31.50	26.2	25.2
7	End of test	3.25	30.25	25.4	25.2
			TEST 12		
0	0	0	31.6	26.6	26.6
1	.85	.58	31.02	26.1	26.1
2	1.48	.85	30.75	25.8	25.6
3	1.97	1.05	30.55	25.6	25.3
4	2.35	1.50	30.10	25.3	24.8
5	2.73	1.88	29.72	25.0	24.6
6	3.05	2.30	29.3	24.6	24.3
7	3.30	2.43	29.17	24.4	24.1
8	3.55	2.54	29.06	24.3	23.8

Note: Water content at trimming = 31.2%
Volume prior to consolidation = 80.0 cc
Specific gravity of solids taken as 2.77

and 10, as is shown dotted in the figure, were assumed, the principal arrangement would be resolved and a dimensionless plot could be produced by dividing the ordinate and abscissa of all points in Figure 2.20 by 8.0 kg/cm^2 (the maximum past consolidation pressure). The resulting plot, it could be hypothesized, would be general for any maximum past pressure.

2.10 Shear strength parameters at constant water content

If the shear stress on the failure plane at the time of failure(τ_{ff}) is plotted above the normal effective stress existing on this plane ($\bar{\sigma}_{ff}$) and this plotting be done for conditions of constant water content at failure, the so-called "true cohesion" (c_e) and "true angle of internal friction" (φ_e) will be obtained (HVORSLEV, 1937). Such a plot, of course, can be done for several water contents at failure. The plot can be made dimensionless by dividing the ordinate and abscissa of each point by the consolidation pressure necessary to produce the same water content in a normally consolidated specimen. If this be done, a single straight line will be obtained having the angle φ_e as its slope and intercepting the y axis at a value $\mathcal{A}$. The best form for such plotting with data similar to that obtained in this test is seen in Figure 2.2. A best fit straight line through these points is drawn and Φ_e and $\mathcal{A}$ calculated as shown in Figure 2.21. With the exception of Tests P-2 and P-3, the line as drawn fits the points quite closely, and this plot seems to afford the best means of generally describing the recorded shear strength behavior of the Loess.

Due to the scatter of data in the consolidation water content plot (Figure 2.16), the following method of determining an appropriate value for p_e was employed: (a) In normally consolidated tests, the actual consolidation pressure was used. The assumption is that void ratio at failure rather than water content is the important criteria in the determination of shear strength and that the void ratio is a function of consolidation pressure regardless of the degree of saturation; (b) Lacking such logical assumptions for the overconsolidated tests, the equivalent consolidation pressure was determined by projecting the point vertically to the rebound line and from this interaction

horizontally to the normal consolidation line. This determination is shown by dotted lines in Figure 2.16. The data for plotting Figure 2.21 are listed in Table 2.3.

2.11 Engineering parameters of shear strength behavior

The usual engineering shear strength plots have been constructed in Figures 2.22 and 2.23. In Figure 2.22 is plotted the shear stress on the failure plane at failure versus the effective stress acting normal to the failure plane at failure. Failure was assumed to occur on a plane represented by the point of tangency of the Mohr's circle of stresses at failure to the resulting failure envelope and when the condition of maximum deviator stress was reached in the test. The plot in Figure 2.22 gives the envelopes to the Mohr's circles of stress drawn in terms of the effective principal stresses existing at failure.

Figure 2.23 presents the undrained shear strength (defined, in this case, as one-half the maximum deviator stress) plotted against the corresponding consolidation pressure existing prior to the start of the test.

2.12 Summary and conclusions

The results of an extensive series of tests on a remolded Loess have been presented. These results have been thoroughly analyzed and ideal behavior patterns have been presented. It is apparent that there is considerable scatter of the data. This scatter, it is felt, is due to difficulty in obtaining homogeneous, saturated test specimens. The observed behavior fits the idealized patterns only fairly well. The discrepancy, it is felt, is due not only to the non-homogeniety and non-saturation of samples, but may also represent some deviation from typical behavior due to an interaction of the behavior patterns of the colloidal and granular fractions.

Chapter 3

RAPID TRIAXIAL COMPRESSION TESTS ON SATURATED LOESS

3.1 Introduction

This chapter contains the description of a series of rapid triaxial compression tests performed upon saturated, normally consolidated samples of Loess. This series of tests was of a preliminary nature, performed in the planning stage of a research program on the nature of possible mechanisms of the effect of rate of strain application upon the stress-strain behavior of saturated soil media.

3.2 Description of the soil

The soil employed in this series of tests was the same soil used in the static triaxial compression tests described in the previous chapter. A complete description of this soil and listing of its engineering properties and mineralogical data can be found in Chapter 2 of this report and in (MIT 1959b).

3.3 Preparation of test samples

The samples of saturated Loess for this series of tests were trimmed from a large "cake" of the soil prepared by consolidation from a slurry in exactly the same manner as were the samples employed in the static triaxial compressions tests described in Chapter 2 of this report. Based on experience gained in the preparation of the previous batch of soil, every possible precaution was exercised to insure that the samples were uniform, homogenous and saturated.

3.4 Consolidation of trimmed test specimens

Trimmed test specimens were placed in a triangle chamber of Norwegian Geotechnical Institute design, modified to accept an appropriate load cell. The specimens were set on the lucite pedestal of the load cell, six saturated vertical filter strips were affixed to the specimens, and saturated porous

stones were placed on top of each specimen followed by lucite top caps having provision for top drainage through connecting lengths of saran tubing which passed through the cell base plates. Each specimen was incased in two thin latex membranes separated by a layer of silicone grease and sealed to the top cap and to the load cell piston by two rubber"o" ring seals.

Following the preparation of each specimen, the triaxial chamber was sealed and filled with previously deaired water, and the consolidation chamber pressure was applied. In all tests of this series, the test specimens were allowed to proceed to 100% of primary consolidation under a chamber pressure of 4.0 kg/cm^2 (56.8 lb/in^2).

3.5 Rapid triaxial compression testing

The test series involved the testing of four identical specimens. Two specimens were tested at a chamber pressure equal to the consolidation pressure, while the other two were tested unconfined (chamber pressure = 0). In both cases, testing was performed with the drainage line closed off (undrained), but in the unconfined tests the chamber pressure was released prior to testing.

Two rates of strain were employed, one fast and one slow, with one of the confined and one of the unconfined specimens being tested at each strain rate. The fast strain rate used was the fastest rate available on the MIT dynamic load frame, 750% per second, while the slow rate was 0.15% per second, as fast as was consistent with visual recording of the axial load by proving ring readings. The fast rate produced failure in a time on the order of 10 milliseconds while several seconds were required to fail specimens using the slow rate. Loading at the slow rate was accomplished using a standard mechanical load frame designed and constructed by Wykeham-Farrance Engineering Ltd. of Bucks, England.

3.6 Instrumentation

The instrumentation for sensing the applied load and resulting deflection of the specimens tested at the rapid rate of strain is, with the exception of the load cell, the same as is fully described in (MIT 1959a). Briefly, the

deflection sensing element is a D.C. strain gage slide wire potentiometer which is capable of sensing deflections in 0.001 inch increments, and the load sensing element of the load cell is a force transducer wherein a bridge configuration of unbonded strain gages senses the minute deflection of a thin steel diaphram. The output of these sensing elements is displayed on an oscilloscope and the trace photographed by means of a Polaroid Land camera attachment.

In the slow test, the output of the sensing elements was plotted directly on a Moseley, Model 4, X-Y Recorder. In Tests 2 and 4, the pen of the X-Y Recorder, which was recording strain, was activated at predetermined proving ring leadings, allowing quite rapid recording of the load deflection data. In addition to the proving ring data, the output of the load cell was recorded in Test 4 allowing a comparison of externally measured loads with those measured inside the triaxial chamber. This procedure allows some evaluation of the possible error in the testing techniques due to piston friction.

3.7 The new load cell

In a discussion in (MIT 1959b), it was pointed out that the load cells originally designed for use with the MIT dynamics testing equipment were found to be moderately sensitive to error due to off center loading and were rather difficult to maintain as the Teflon membrane was prone to develop leaks, and the replacement procedure was complicated. When a new design force transducer (Dynamic Instrument Co., Carlton Street, Cambridge 39, Mass., Model FT) became available, a new approach to the load cell problem was possible. The load cell described in this section is the first constructed using the force transducer. Since this series of test, several variations of the basic load cell have been constructed.

The new load cell, pictured in Figure 3.1, has been constructed upon a base similar to those employed in the old load cells so that it can be used in the MIT modified N.G.I. triaxial cells. Any horizontal component of load will be resisted by a normal force between the lucite piston and the Teflon, is almost frictionless. Thus the force transducer senses only the vertical component of

the load applied to the piston. Prior to use, this load cell was carefully calibrated against the proving ring employed in the tests at the slow rate of strain. In addition, in order to investigate the possibility of any "strain-rate effect" inherent in the load cell, it was loaded by means of a controlled deflection of a calibrated spring at rates of loading representing the complete range involved in dynamic soil testing. The cell was found to be free of any such effect.

3.8 Results of rapid triaxial compression tests on saturated Loess

The stress vs. strain data recorded from this series of triaxial compression tests on saturated Loess have been reduced and plotted in Figure 3.2 and 3.3. The loads as obtained from either the proving ring reading or the load cell output, were divided by an area corrected for axial strain to obtain the stresses while the deflections were divided by a length of sample calculated to exist following consolidation. These calculations were made on the following assumptions: (a) water content at trimming equals 32.1% and the volume as trimmed equals 80 cc; (b) the specific gravity of solids, $G_s = 2.77$; (c) following consolidation the water content equals 27.3% (See Figure 2.16); (d) unit strain during consolidation was the same in principal strain directions (i.e., isotropic soil structure); and (3) during compression testing, the area is given by the standard relationship assuming cylindrical deformation , $A_\varepsilon = A_o \frac{1}{1-\varepsilon}$, where A_ε = corrected area at any strain level, A_o = area following consolidation and ε = unit strain.

Assuming a "static strength" of 30 lb/in^2, based on the idealized picture of the behavior of the Loess presented in Figure 2.19, the plot of increase in strength over the static strength vs. the time of loading, Figure 3.4(a), has been constructed. In this plot and the following plot, Time of Loading has the modified definition adopted in (MIT 1959b) (i.e., time to 1% strain) making it a direct measure of the rate of strain.

In Figure 3.4 (b) the modulus to 1% strain has been plotted against Time to Failure previously defined. The static modulus to 1% strain was obtained from Test 14 of the static triaxial test series described in Chapter 2.

3.9 Discussion and analysis of results of rapid triaxial compression tests on compression tests on saturated Loess

The following discussion is an attempt to develop some picture of the interrelationship of the various mechanisms possibly contributing to the manifestations of strain-rate effect on the stress vs. strain behavior of saturated samples of fine grained soils tested in triaxial compression. The analysis will undoubtedly oversimplify the behavior of this particular soil in which interaction between the silt sized bulk of the particles and their colloidal matrix complicate not only the dynamic response, but, as has previously been pointed out, the static response aswell.

It is conceded by many, but by no means all, of the investigators in the shear strength aspect of soil mechanics research, that the strength of a fine grained soil consists of two components, one dependent upon the relative-spacing of soil particles at failure, as indicated by the void ratio, and the other dependent upon the effective stress acting between these particles. At the writing of this research report, the best that can be said is that for any failure water content there exists a unique shear strength vs. effective stress relationship.

A fine grained soil depends, for this shear resistance and effective stress relationship, upon its structure, where structure is defined as the joint contribution of particle orientation brought about by the forces acting between particles and by these interparticular forces themselves. In a saturated soil, if $\tau = f(\bar{\sigma}) = f(\sigma - \mu)$ (i.e., shearing resistance = function of the total stress minus the pressure in the fluid phase), then changes in structure can contribute to changes in this relationship either by altering the strength-effective stress relationship or by affecting the manner in which pore water pressure is developed by the applied stresses and thus altering the effective stress at failure.

Both the manner in which the structure of a fine grained soil resists shear stress applications and the manner in which various components of this structural resistance react to changes in rate of strain give an ideal fine grained soil its typical strain-rate behavior pattern.

If pore pressure considerations are temporarily overlooked, a first step in understanding ideal behavior can be made. This step involves an idealization of viscous vs. brittle behavior patterns as discussed in (MIT 1959b). Briefly, a viscous strain-rate behavior pattern is one as idealized in Figure 3.5a in which an increase in strain-rate increases the modulus of the stress vs. strain curve, while an idealized brittle display is one in which the stress strain curve rises sharply to a peak and an increase in the rate of strain causes simply an elevation of this peak with no basic change in modulus. In soils, brittle behavior may be characteristic of a soil structure in which there is an actual bonding or linkage between particles. The modulus of the stress vs. strain curve is related to the rigidity of an individual bond and hence is not effectively a function of strain-rate, while an increase in rate of strain can statistically affect the number of bonds active at peak stress and thus raise the peak. Viscous behavior, on the other hand, could be expected to occur in a soil where parallel particle orientation leads to a structure whose strength arises from forces acting between particles and thus could be typically viscous in nature. Brittle behavior could be expected in a soil having what has been characterized as a flocculated structure as would exist in normally consolidated clays with the appropriate formation environment or in clays compacted wet of optimum water content could be expected to display viscous strain rate behavior.

In an actual soil, the development of pore water pressure during the application of shear stresses adds another complicating factor to the already complicated picture. Pore pressures set up due to application of shear stresses can best be described in terms of the pore pressure parameter A (SKEMPTON, 1954), where A is defined as $\frac{\Delta u}{\Delta (\sigma_1 - \sigma_3)}$ (i.e., the ratio of change in pore pressure during the application of a particular deviator stress increment to this deviator

stress increment. In a saturated specimen, tested in triaxial compression, two mechanisms by which rate of strain could influence the pore pressure and thus affect the shearing resistance are: (1) the change in A at a point in the specimen due to an increase in rate of strain; and (2) change in overall A value for the specimen as a whole due to the effect of migration of pore water to or away from the zone in which failure is taking place. As time is required for the migration of pore water, this becomes a time dependent phenomenon.

Mechanism 2 is, of course, not fundamental as it has its roots in the stress distribution in a triaxial compression specimen. This stress distribution is little understood. BISHOP, BLIGHT and DONALD (1960), in a study of the effect of rate of strain on base pore pressure measurements, have described this mechanism in the following manner:

The unequal distribution of stresses in a triaxial specimen occurs due to end restraint at the base and at the cap. End restraint has the effect in these regions of increasing σ_1 slightly and considerably reducing the deviator stress $(\sigma_1 - \sigma_3)$. The basic pore pressure equation $\Delta u = B\,[\Delta\sigma_3 - A(\Delta\sigma_1 - \Delta\sigma_3)]$ can be rearranged in the form $\Delta u = B[\Delta\sigma_1 - (1-A)(\Delta\sigma_1 - \Delta\sigma_3)]$. Both effects of end restraint will increase Δu in the end regions unless $A > 1$. If the test is run slowly enough, the pore pressure throughout the sample will be equalized by a flow of water within the sample. This flow will be seen to decrease the strength at the mid-portion of the sample if $A < 1$ and possibly increase it slightly if $A > 1$. Therefore, if $A < 1$, an increase in strength should occur if the test is run rapidly enough to prevent the migration of pore water, while if $A > 1$, the possibility of a slight decrease in strength exists.

Mechanism 1, the altering of the A value of any element of the soil is much more fundamental and reflects the nature of the soil structure. A possible mechanism of this alteration is shown in Figure 3.5(c). In the structure shown, the bonds at A are assumed to be somewhat viscous in nature.

Under a slow stress application, the diagonal particle translates as the viscous contact at A permits this to occur. As this translation proceeds, some of the forces maintaining equilibrium of particle spacing are disturbed, a tendency for collapse and thus development of positive pore water pressure ensues. However, under a rapid application of load, the viscous behavior at the contacts at A form, in effect, a hinge. Thus there exists a tendency for rotation to occur which in the extreme, could lead to the development of a negative pore water pressure. This mechanism would therefore lead to an increase in strength as the rate of strain is increased.

With these points in mind, an anlysis of the rapid tests on the saturated Loess may be undertaken. It is important to remember that these tests were of a very preliminary nature, and hence the following discussion represents more the manner in which such analyses may be made rather than positive conclusions regarding this saturated Loess.

The results of the unconfined compression tests are plotted in Figure 3.2. This soil tested in unconfined compression exhibits a strain rate effect on maximum shear strength of about 10%. This stress-strain behavior is indicative of behavior intermediate between viscous and brittle as both a general steepening of the stress vs strain curve and an elevation of peak stress appear. As the mode of failure of unconfined compression tests is probably quite different from that of confined tests, little here can be learned regarding structure. Unconfined tests probably fail due to splitting of the sample. This splitting induces a negative pore water pressure which, according to the magnitude it develops, controls the shear strength.

In Figure 3.6 is plotted a straight line representing the relationship between shear strength and effective minor principal stress at failure for a water content of 27.3%. This plot has been constructed by expanding Figure 2.21 for an equivalent consolidation pressure of 56.8 lb/in^2. If

the deviator stress at failure be plotted on this line, the effective minor principal stress at failure can be estimated. In these unconfined tests, the total minor principal stress is zero, and thus the pore pressure at failure can be deduced. These pore pressure at failure give a clue to the probable cause of the strain rate effect in the unconfined specimens. The slow test failed at a deviator stress corresponding to a pore-water pressure of 15.5 lb/in^2 below atmospheric pressure. This is substantially the value at which caviatation or vaporization of free water occurs at room temperature. In order to cavitate, nucleation must occur, and a site for nucleation must be found. Statistically, the search for a nucleation site is time dependent, and water could be expected to obtain an absolute tension in a rapidly loaded specimen. Other phenomena substantiating this expectation have been noted (see WHITMAN, RICHARDSON and HEALY, 1961). The deduced pore pressure at failure of 21.2 lb/in^2 below atmosphere in Test 1, the rapid test, then, is the result of the rapid application of stress and gives rise to the strain rate effect in this situation.

The results of the confined tests can be analyzed in a similar manner. The stress vs strain curves as plotted in Figure 3.3 hint at brittle behavior. Both the slow and fast tests yield shear strengths exceeding the assumed static strength by approximately 40%. However, the fast test yielded a strength about 5% lower than the slow test. Hence, the overall strength increase over the static strength can be assumed as pore pressure behavior attributable to mechanism 1, while the decrease in strength from the slow to the fast rate could be attributable to mechanism 2, since the static A value for this soil is greater than 1. However, it is equally possible that this decrease in strength is due to a scatter in test results and is not a true behavior characteristic of the soil.

3.10 Piston Friction

Figure 3.3 presents interesting data on the possible influence of piston friction in tests where the load is read externally on a proving ring. Test 4 was performed reading the load externally on a proving ring

but also sending the load inside the triaxial chamber using the load cell. As is apparent, a possible piston friction effect of 10% can occur. However, this test was quite extreme in that the chamber used was the one customarily employed in the fast tests on the M.I.T. rapid load frame and was known to have a rather rough fitting piston.

3.11 Conclusions

The results of a series of a triaxial compression tests performed at rapid rates of strains have been presented. The data obtainable from this series of tests is summarized in Figure 3.4, but it is cautioned again that this series of tests was of a preliminary nature. Possible mechanisms accounting for strain rate effect in fine grained soils have been presented and discussed and the results of this series of tests have been analyzed in the light of these mechanisms.

It was concluded in Chapter 2 of this report that the Loess greatly deviated from ideal in its static stress vs. strain behavior. This complication of behavior makes the interpretation of these dynamic test results quite difficult. On the basis of these preliminary tests on the Loess, it has been decided to concentrate research efforts on the Fat Clay until better techniques of testing and analyzing results can be developed.

In particular, before returning to rapid tests on the saturated Loess, it is deemed necessary to: (a) gain new understanding of the behavior of a predominantly fine grained soil such as the Fat Clay, and (b) develop the necessary techniques to determine experimentally the various levels of pore pressure obtained in these rapid tests.

Chapter 4

RAPID TRIAXIAL COMPRESSION TESTS ON SATURATED FAT CLAY

4.1 Introduction

This chapter describes a series of rapid triaxial compression tests on a saturated fat clay. This series of tests was of a preliminary nature, and, as with the rapid triaxial compression tests on the saturated Loess, was performed as a part of the planning stage of an extensive program investigating strain rate effects in saturated soils. A total of four tests were performed, 2 normally consolidated and 2 overconsolidated. Two strain rates were employed, one very rapid one and one slow, with one specimen of each stress history being tested at each strain rate. The results of these dynamic tests are compared with known behavior patterns for this soil obtained from previously performed static tests.

4.2 Soil specimens

The soil employed in this series of tests was the Fat Clay employed in the static triaxial compression tests described in Chapter 5 of (MIT 1959b). The individual test specimens were trimmed from prisms of soil from Batch 3 as described in (MIT 1959b) and stored in oil. Batch 3 was consolidated in June of 1959.

The testing of specimens from this batch at static rates was undertaken in July of 1959. This series of dynamic tests was performed in November and December of 1959. The possible effect of this storage period is unknown at this time. However, concurrent studies at MIT indicate that storage time differences of this magnitude influence comparison of test results only to a minor degree.

4.3 Triaxial consolidation

Following trimming the specimens were placed in NGI triaxial cells following exactly the same procedure used for the tests on the Loess and

described in Chapter 3 of this report. Two samples were normally consolidated to 60 lb/in^2 in three pressure increments.

The two overconsolidated specimens were normally consolidated to 120 lb/in^2 in four pressure increments and then allowed to rebound to 15 lb/in^2. It was originally intended in this test program that the stress history prior to testing be such that all specimens would arrive at the same water content. Considerable difficulty was experienced in maintaining the 120 lb/in^2 consolidation pressure, and on two occasions this pressure was lost overnight, and had to be restored in the morning. As a result of this cycling of consolidation pressures, the over-consolidated specimens arrived at a water content a good deal lower than that anticipated.

4.4 Rapid triaxial compression testing

Following consolidation, the specimens were transferred from the cell in which they were consolidated into another NGI triaxial cell having a load cell in the base. This series of tests was performed prior to the rapid triaxial compression tests on the Loess and hence prior to the construction of the load cell described in Chapter 3. The load cell employed in this series of tests was the medium capacity load cell described in (MIT 1959a).

Tests were performed on the MIT dynamic load frame (MIT 1959a) at the two extreme rates of strain which this device affords. The fast tests employed a rate of strain of 12 inches/second while the slow rate was 0.1 inches/second.

The instrumentation for sensing and recording the load-deformation behavior was that described in (MIT 1959a).

4.5 Results of rapid triaxial compression tests on the fat clay

The stress vs strain behavior obtained in this series of four tests is plotted in Figures 4.1 and 4.2. In addition, the results of static test M-8 from the series of static triaxial compression tests recorded in (MIT 1959b) has been replotted. No overconsolidated static test is directly comparable to the dynamic tests plotted in Figure 4.2 so no such static curve is plotted. The stress levels were computed using the recorded load and corrected areas computed in the manner discussed in section 3.8 of this report but using the water contents appearing in Table 4.1. It is interesting to note that the lengths at the end of consolidation computed on the basis of the assumption of isotropic unit strain compare quite closely with lengths carefully measured at this time. This comparison is made in Table 4.1.

Figure 4.3 is a reproduction of the water contents consolidation pressure data for Batch 3 of the Fat clay appearing in (MIT 1959b).

A static strength value was obtained directly from test M-8 in the case of normal consolidation and deduced as will be described in the case of the overconsolidated specimens. The ratio of strength increase over this static value is plotted against time to failure in Figure 4.4a. The pore pressure parameter A at failure, deduced as will be described, is plotted against time to failure in Figure 4.4b. In both these instances, time to failure has the modified definition of time to one percent strain, as described in (MIT 1959b).

4.6 Analysis and discussion of results of rapid triaxial compression tests on the fat clay

A study of Figures 4.1 and 4.2 can give some insight into the role that the type of structure plays in determining the shearing resistance repose pattern, and the relationship of each to rate of strain. The stress vs strain response patterns of the normally consolidated samples rise sharply to peaks. The effect of an increase in the rate of strain on these

response patterns is to elevate the peak strength with no substantial change in initial modulus. This "brittle" behavior is indicative of a soil structure tending toward the "flocculated" type. In contast, the overconsolidated specimens plotted in Figure 4.2 display behavior patterns in which the effect of an increase in rate of strain is to increase the shear strength both by an elevation of the peak value and by a substantial increase in the modulus or slope of the early portion of the stress vs strain curve. This type of behavior containing elements of both brittle and viscous strain rate characteristics is indicative of an effect of a structure tending toward a dispersed or oriented particle arrangement but retaining a considerable degree of random or "flocculated" arrangement. Hence it may be assumed that the stress history leading to the overconsolidated state attained in this series of tests tends to destroy some of the elements of the flocculated structure present in the normally consolidated specimens with a resulting improvement of the relative degree of particle parallelism.

A discussion of the modes of structural contribution to the strain rate effect is included in Section 3.9 of this report. The plot of strength increase over static vs time of loading in Figure 4.4a gives further evidence of the viscous vs brittle aspects of structural behavior. The normally consolidated specimens show a strain rate effect the major portion of which occurs quite rapidly as the fast rate is approached. The increase in strength with strain rate in the overconsolidated specimens, however, occurs gradually.

The rapid increase in the first instance is what would be expected from brittle structural behavior, while the second situation is highly indicative of elements of viscous behavior.

In Figure 5.8 of (MIT 1959b) is presented a Hvorslev Parameter Plot for the fat clay which yielded a true angle of internal friction (φ_e) = $11\frac{1}{2}^\circ$ and a true cohesion (c_e) = 0.14 p_e where p_e is the pressure which would produce the particular water content in a normally consolidated sample. Subsequent work at MIT indicates that a more reasonable value may be $\varphi_e = 17.1^\circ$ and $c_e = 0.115\ p_e$.

The best estimate of the static strength in the overconsolidated tests was arrived at by assuming an A at failure (where $A = \frac{\Delta u}{\Delta(\sigma_1 - \sigma_3)}$) of 0 (which corresponds to tests M_4 and M_{14} in M.I.T. 1959b. These tests have the same nominal stress history as those in the current series). Then, σ_3 at failure = 15 lb/in^2. Using $\varphi_e = 17.1$ and $c_e = 0.155$ gives:

$$\alpha = \text{Tan}^{-1} \frac{\text{Sin } \varphi_e}{1-\text{Sin } \varphi_e} = .416 \text{ and } b = \frac{c_e}{p_e} \times \frac{\text{Cos } \varphi_e}{1-\text{Sin } \varphi_e} = .210$$

(see Figure 5.8 of M.I.T. 1959b). For a failure water content of 30.5% $p_e = 6.83$ kg/cm^2 (Figure 4.3). Therefore $(\sigma_1 - \sigma_3)$ at failure = $b\, p_e + \bar{\sigma}_3 \text{ Tan}\alpha = 53.4$ lb/in^2.

Using these same values for the Hvorslev parameters (i.e. $\varphi_e = 17.1^\circ$ and $\frac{c_e}{p_e} = 0.155$), the values of σ_3 and thus u at failure can be computed in a similar manner: ($u = \sigma_3 - \bar{\sigma}_3$). These calculations are tabulated in Table 4.1 and lead to the A at failure values plotted in Figure 4.4b. Included in Section 3.9 of this report is some discussion of the manner in which pore pressure buildup and pore pressure distribution in triaxial compression specimens are affected by a change in the rate of strain and thus contribute to the overall strain rate effect. To summarize, two possible mechanisms were suggested. Mechanism 1 is the change in A in elements of the soil sample due to an increase in the rate of strain, while Mechanism 2 is a change in the overall A value of the specimen due to a flow of water to or from zones of different stress conditions.

Some deductions regarding the mechanisms responsible for the pore pressure changes with increased rate of strain may be made by: (1) looking at the rearrangement of the basic pore pressure equation given in Section 3.9: $\Delta u = B[\Delta\sigma_1 - (1-A)(\Delta\sigma_1 - \Delta\sigma_3)]$; (2) noting that restraint at triaxial specimen ends will tend to increase σ_1 and considerably reduce $(\Delta\sigma_1 - \Delta\sigma_3)$ over values in the mid-portion; (3) and observing in this equation that, if $A > 0$ (as in a normally consolidated clay) the pore pressure at the base will still be of the same order as that at the middle, while if $A < 0$, there exists the possibility that, in a rapid test, a considerably less negative, or even positive pore pressure could be developed close to the ends with a negative pore pressure in the remainder of the sample.

TABLE 4.1

DATA FROM TESTS AND CALCULATIONS, FAT CLAY

Test	ω at Trimming	ω at Failure	Stress History	$\frac{\sigma_1-\sigma_3}{2}$ Max.*	e*	Calculated* $\bar{\sigma}_3$	σ_3*	u*	A_f	Following Consolidation: Measured Length	Following Consolidation: Calculated Length
1	50.9	36.5	NC	27.8	54.1	39.5	60	20.5	+.37	2.952"	2.96"
2	50.7	36.2	NC	20.1	56.2	20.2	60	39.8	+.99	2.953	2.96
3	5.16	30.5	OC	49.7	97	71	15	-56	-.56	2.86	2.87
4	50.3	30.5	OC	36.7	97	40	15	-35	-.48	2.86	2.90
M8	--	--	--	18.7	56.8	16.5	568	40.3	+1.07	--	--

*Stresses in lb/in^2

In a normally consolidated sample with $A \leq +1$ it can be expected that somewhat higher pore pressures will exist in the regions of end restraint than in the center portion of the sample. However, it is felt that the small flows necessary to equalize these differences will have little effect on the average pore pressures at equilibrium, so that slight, if any, strain rate effects due to this pore pressure mechanism 2 would result.

In the overconsolidated sample, it is conceivable that, if a test be run rapidly enough to prohibit any equalization of pore pressures, a less negative (or even positive) pore pressure would exist at the regions of end restraint than in the central portion. Very little flow would seem to be required to substantially increase (make less negative) the pore pressure in this central portion since volume change is taking place on a rebound or reconsolidation portion of the water content vs effective stress curve considerably flatter than the normal consolidation portion. Hence, if the test be slowed to a rate allowing this equalization in pore pressure to occur, Mechanism 2 will operate to reduce the strength.

Following this reasoning, the change in pore pressures due to increase in rate of strain in the normally consolidated specimens which occurs rather abruptly, can be adjudged to be mainly due to Mechanism 1 while the rather gradual increase in the case of overconsolidated specimens can be adjudged to result from the presence of both mechanisms.

4.7 Conclusions

Since a very limited number of tests were performed and these were of a preliminary nature, no definite conclusions regarding the magnitude or nature of the strain rate effect can be drawn. However, knowing that the behavior of this soil is consistent, and follows predictable patterns, it is felt that the best initial approach to an understanding of the strain rate effect in saturated soils lies in a comprehensive study of this soil under dynamic load conditions.

In addition, it has become clearly apparent in these tests that analysis of data, in terms of effective stresses, is extremely important and that development of effective techniques and devices for pore pressure measurements in rapid tests cannot be stressed enough.

SUMMARY OF CONCLUSIONS

Conclusions

1. The results and analysis of an extensive series of "static" triaxial tests on a remolded Loess have been presented. Due to considerable scatter of the data (probably caused by non-homogeneous and not fully saturated test specimens and deviation from idealized patterns of the colloidal and granular factors), interpretation of these dynamic test results on the Loess was quite difficult.

2. The triaxial compression tests on the Loess performed at rapid rates of strain cannot be fully analyzed until the discrepancies in the "static" tests are removed. However, possible mechanisms accounting for strain rate effect in fine grained soils have been analyzed in the light of these mechanisms. On the basis of these preliminary tests on Loess, it has been decided to concentrate research efforts on the Fat Clay until better techniques of testing and analyzing results can be developed.

3. The behavior of the saturated clay in the triaxial compression tests at rapid rates of strain was consistent and followed predictable patterns. It is felt, therefore, that the best initial approach to an understanding of the strain rate effect in saturated soils lies in a comprehensive study of this soil under dynamic load conditions. Since a very limited number of tests were run in this series of preliminary tests, no definite conclusions regarding the magnitude or nature of the strain rate effect can be drawn.

Future Research

A comprehensive study of the saturated clay under dynamic load conditions is now underway. Results of the tests presented in this report have made it increasingly apparent that analysis of data in terms of effective stresses must be emphasized and that effective techniques and devices for pore pressure measurements in rapid tests are essential.

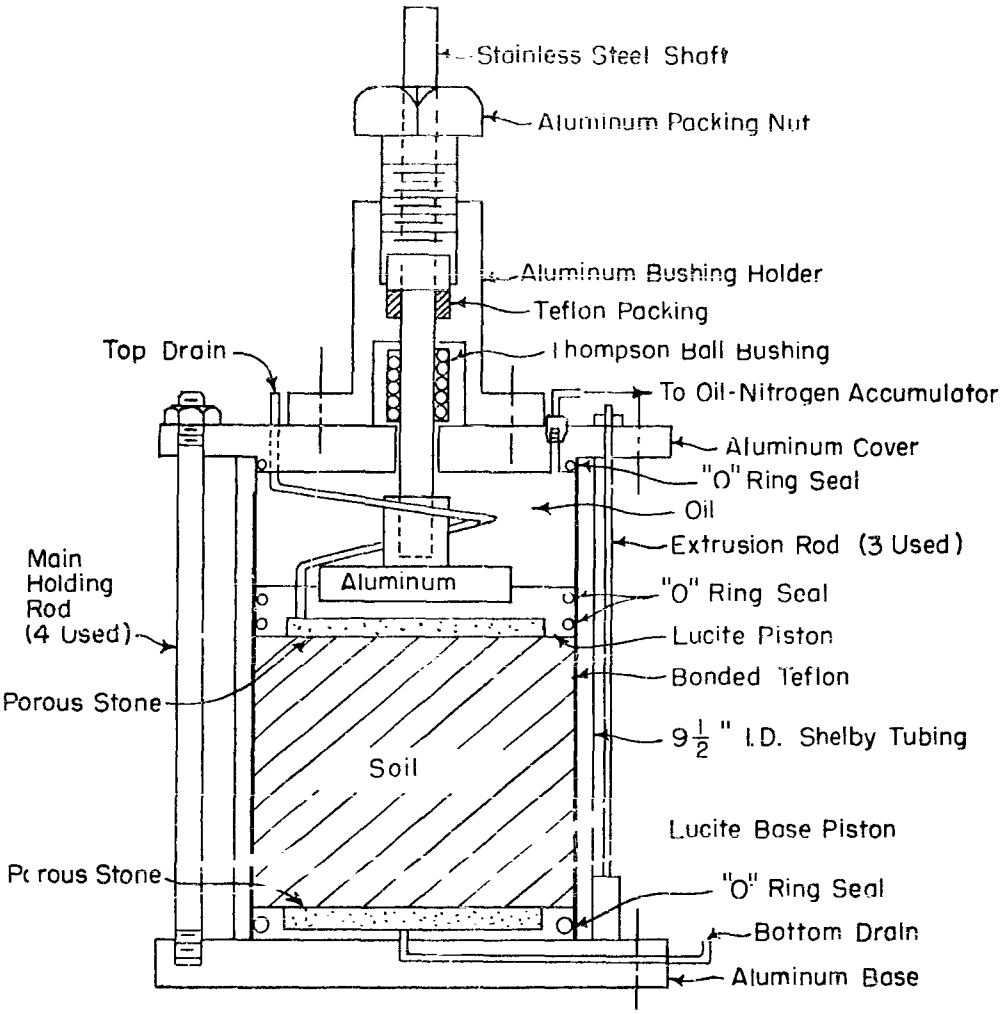

Note: To extrude, relieve pressure, invert consolidometer; remove main holding rods and tighten extrusion rods. Reapply light pressure sufficient to extrude.

FIGURE 2.1 SELF EXTRUDING CONSOLIDOMETER

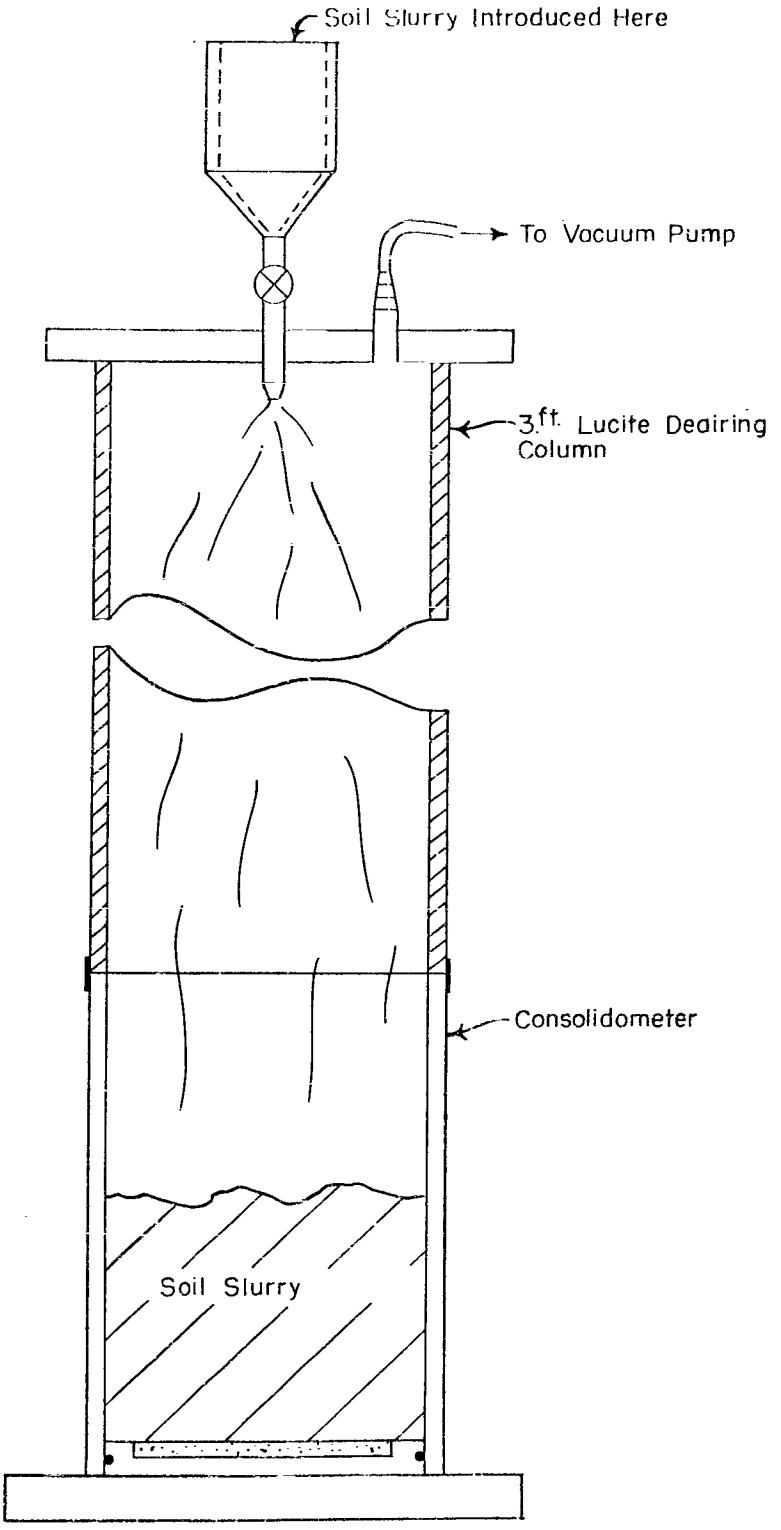

FIGURE 2.2 METHOD OF SLURRY PLACEMENT

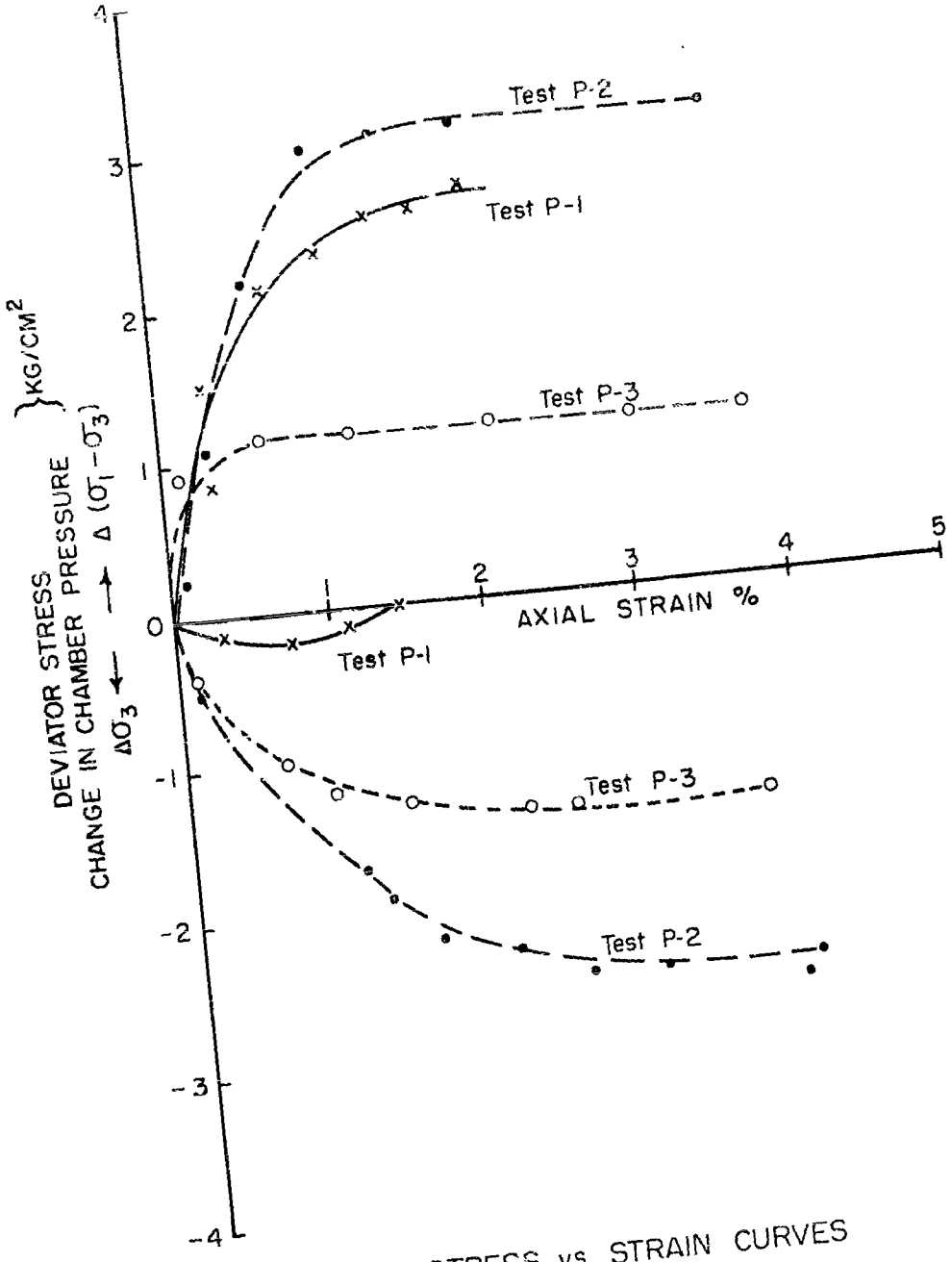

FIGURE 2.3 STRESS vs STRAIN CURVES
PRELIMINARY TESTS

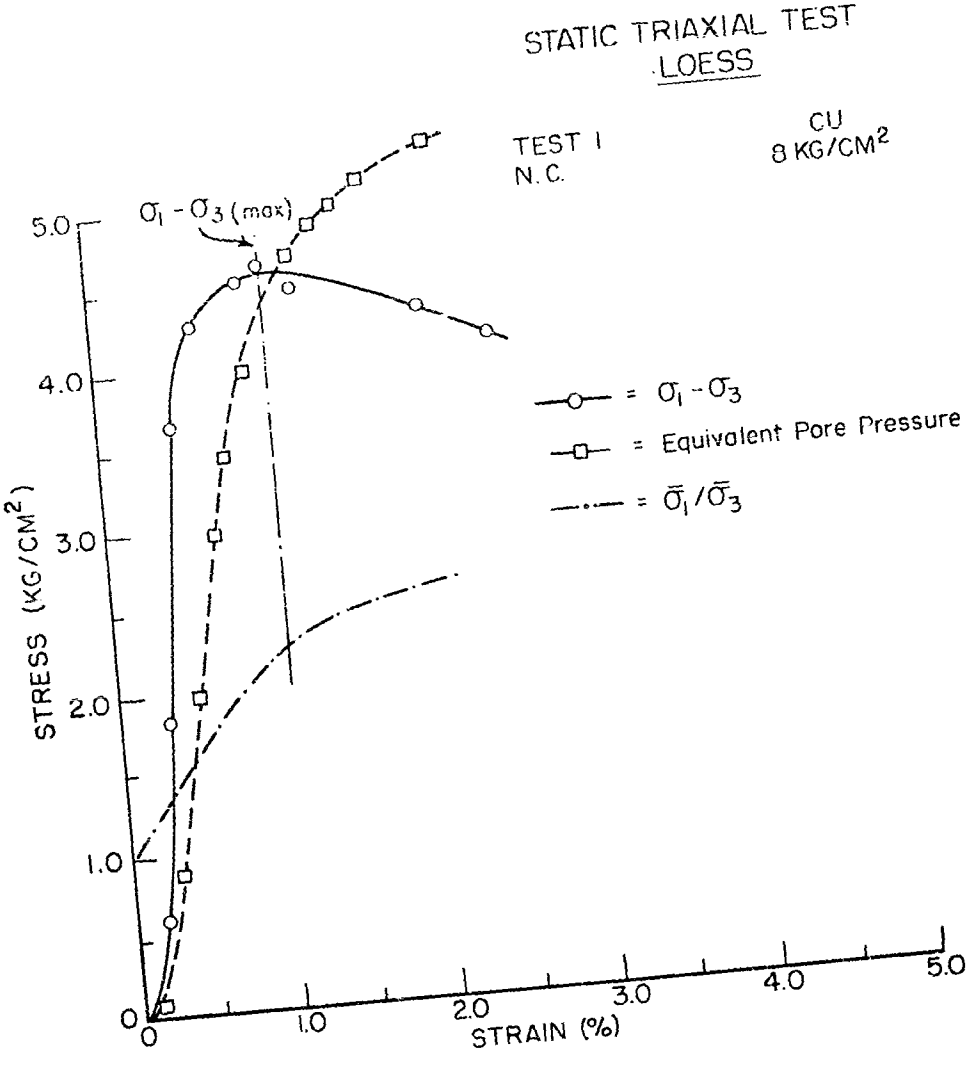
STATIC TRIAXIAL TEST
LOESS
TEST I
N.C.
CU
8 KG/CM2
σ1 - σ3 (max)
5.0
4.0
3.0
2.0
1.0
0
STRESS (KG/CM2)
= σ1 - σ3
= Equivalent Pore Pressure
= σ̄1/σ̄3
0
1.0
2.0
3.0
4.0
5.0
STRAIN (%)

FIGURE 2.4

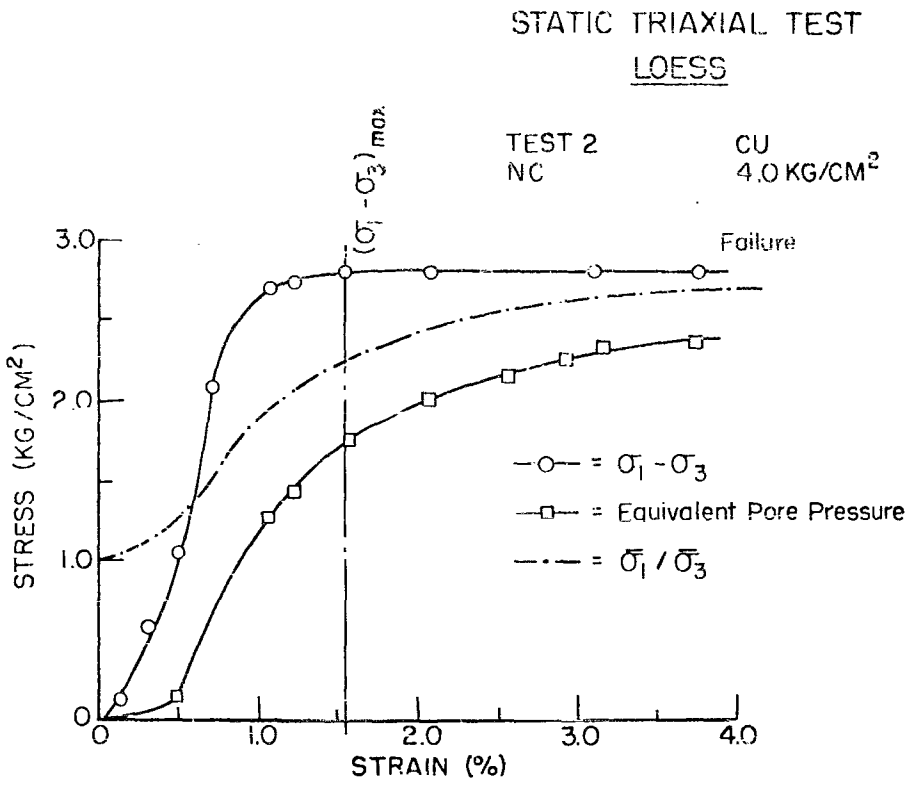
STATIC TRIAXIAL TEST
LOESS
TEST 2
NC
CU
4.0 KG/CM²
Failure
$(\sigma_1-\sigma_3)_{max}$
STRESS (KG/CM²)
STRAIN (%)
$\sigma_1-\sigma_3$
Equivalent Pore Pressure
$\bar{\sigma}_1/\bar{\sigma}_3$

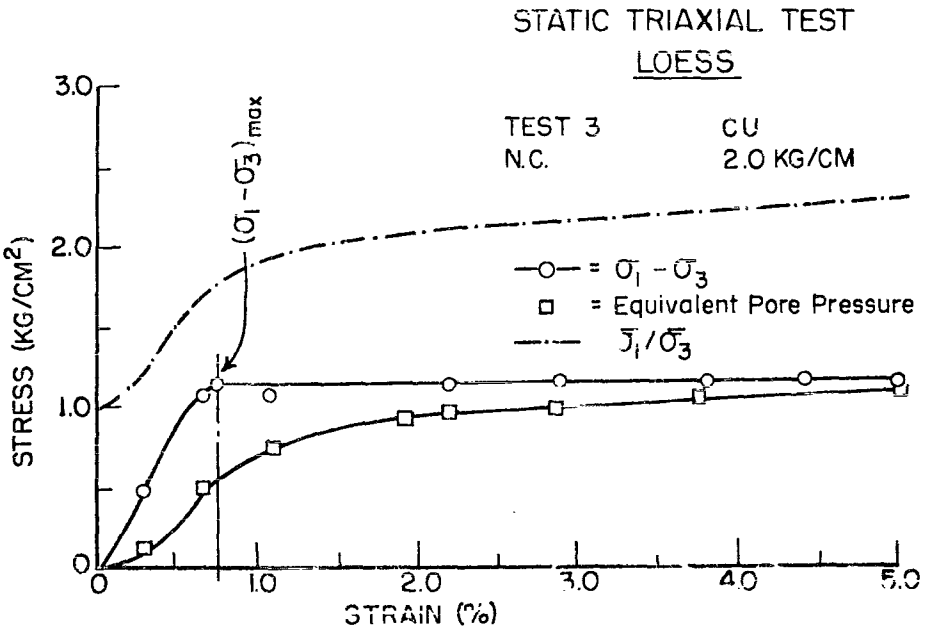
STATIC TRIAXIAL TEST
LOESS
TEST 3
N.C.
CU
2.0 KG/CM
$(\sigma_1-\sigma_3)_{max}$
STRESS (KG/CM²)
STRAIN (%)
$\sigma_1-\sigma_3$
Equivalent Pore Pressure
$\bar{\sigma}_1/\bar{\sigma}_3$

FIGURE 2.5

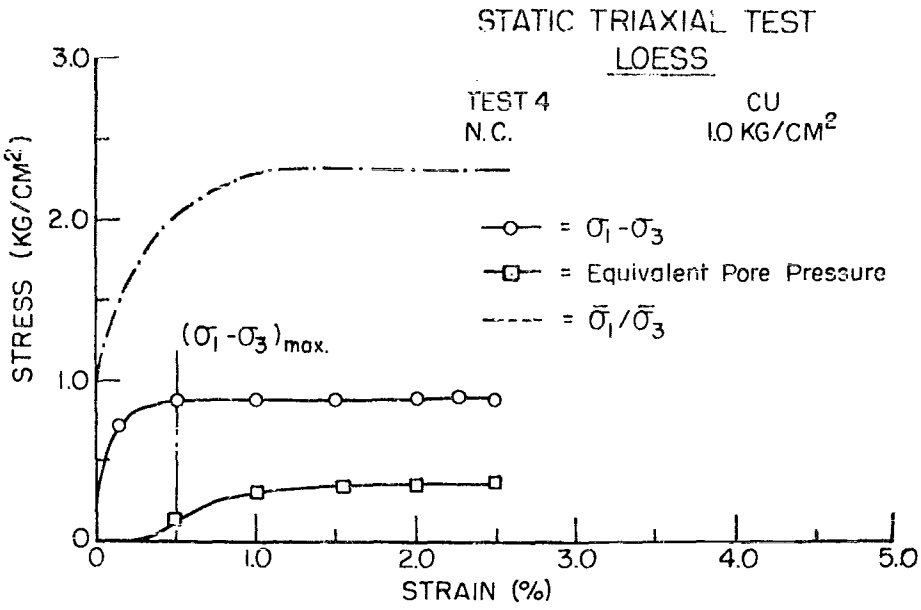
STATIC TRIAXIAL TEST
LOESS
TEST 4
N.C.
CU
1.0 KG/CM2
= σ1 -σ3
= Equivalent Pore Pressure
= σ̄1/σ̄3
(σ1 -σ3)max.
STRESS (KG/CM2)
STRAIN (%)
0
1.0
2.0
3.0
4.0
5.0

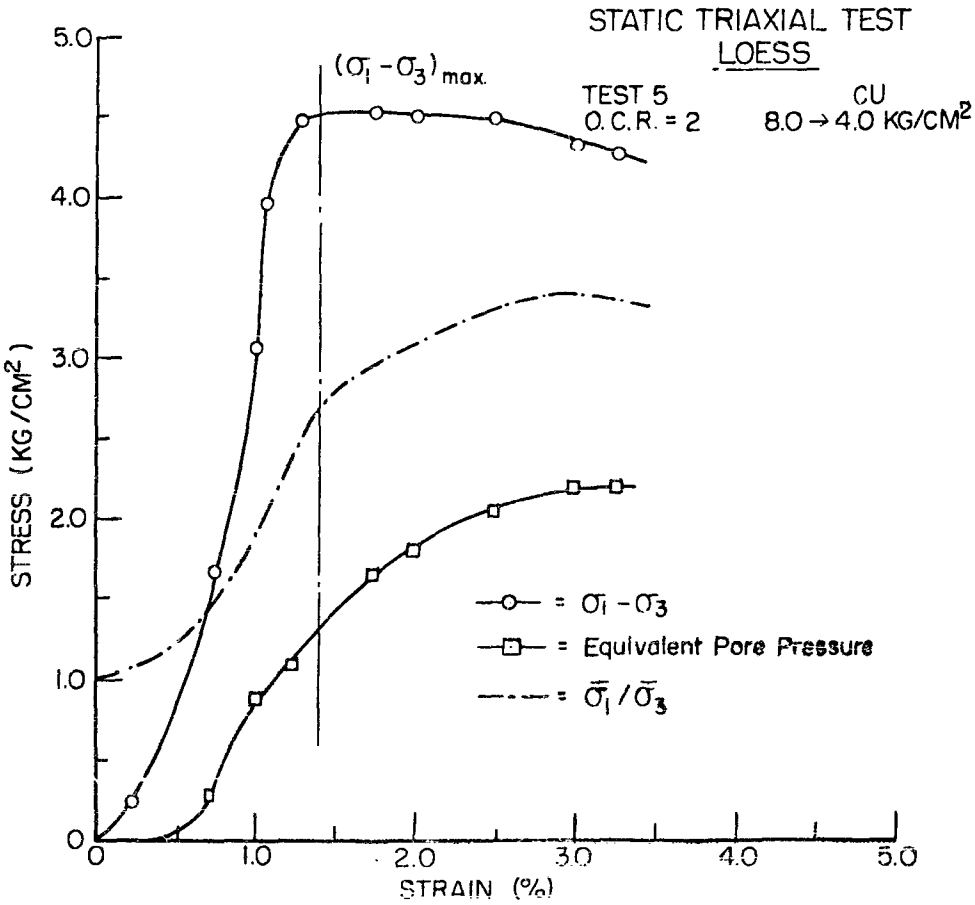
STATIC TRIAXIAL TEST
LOESS
(σ1 -σ3)max.
TEST 5
O.C.R. = 2
CU
8.0 → 4.0 KG/CM2
= σ1 -σ3
= Equivalent Pore Pressure
= σ̄1/σ̄3
STRESS (KG/CM2)
STRAIN (%)
0
1.0
2.0
3.0
4.0
5.0

FIGURE 2.6

STATIC TRIAXIAL TEST
LOESS

TEST 6 CU
OCR = 8 8→100 KG/CM^2

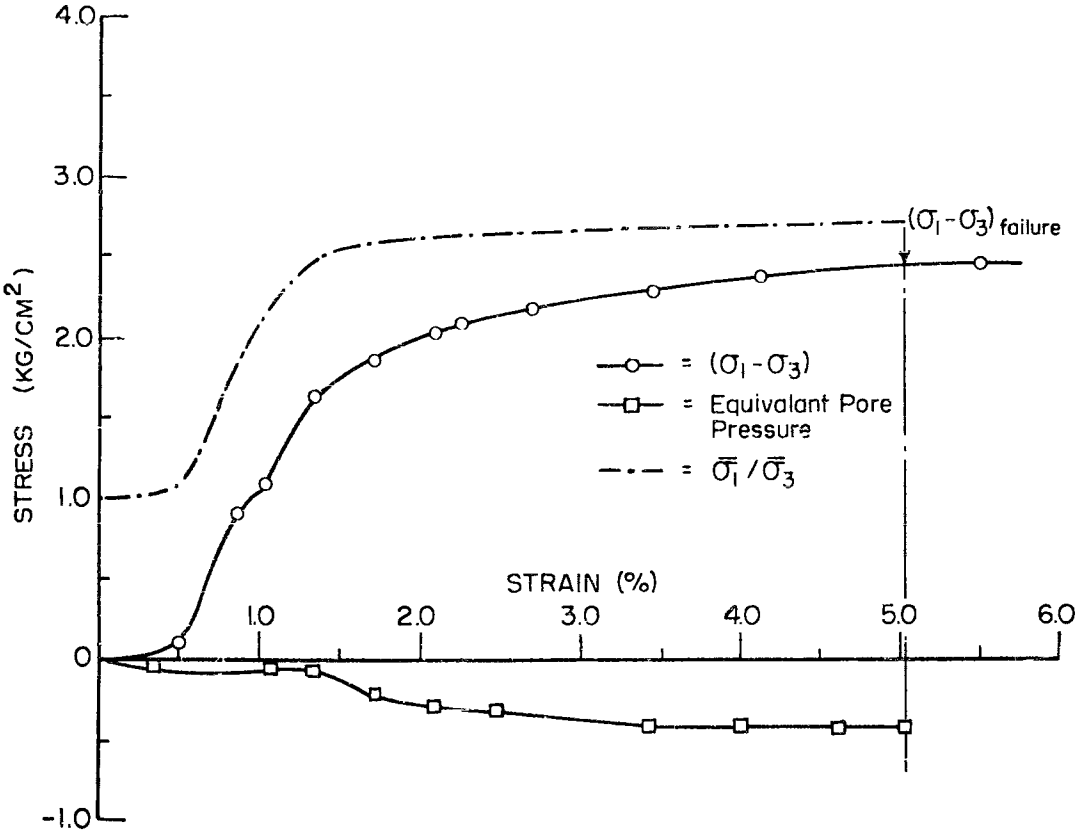

FIGURE 2.7

STATIC TRIAXIAL TEST
LOESS

TEST NO. 7 CU
O.C.R. = 4 8.0→2.0 KG/CM^2

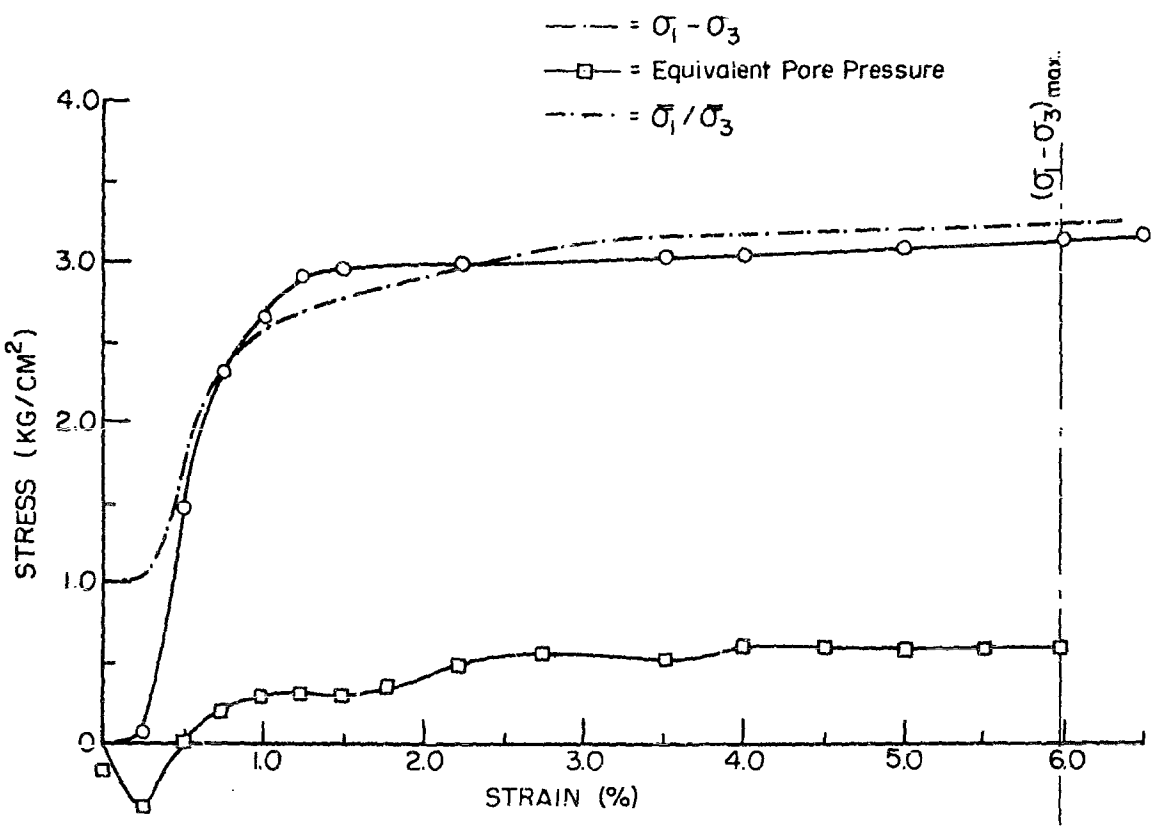

FIGURE 2.8

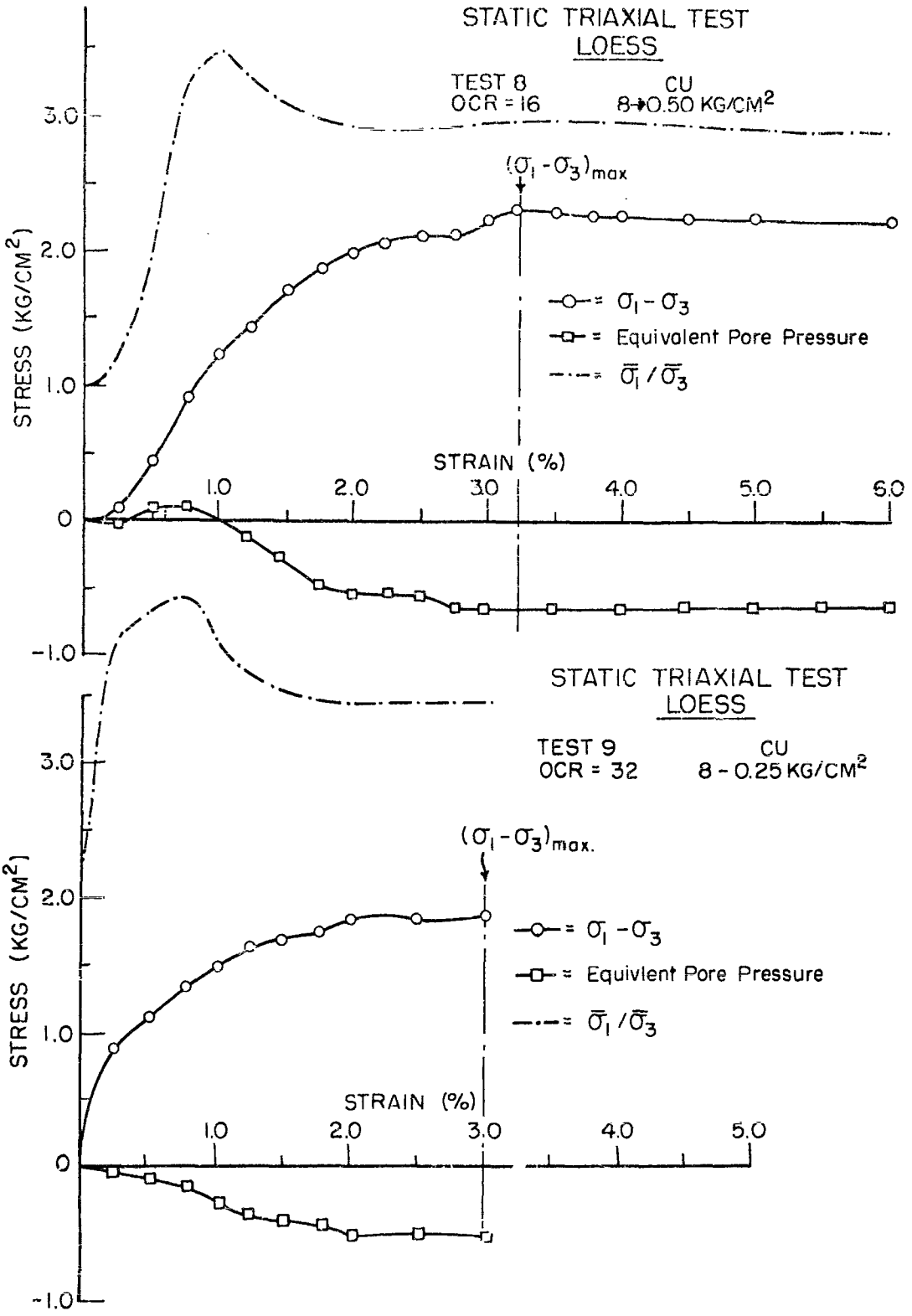
STATIC TRIAXIAL TEST
LOESS
TEST 8
OCR = 16
CU
8→0.50 KG/CM²
(σ1 - σ3)max
σ1 - σ3
Equivalent Pore Pressure
σ̄1 / σ̄3
STRESS (KG/CM²)
STRAIN (%)
3.0
2.0
1.0
0
-1.0
1.0
2.0
3.0
4.0
5.0
6.0
STATIC TRIAXIAL TEST
LOESS
TEST 9
OCR = 32
CU
8 - 0.25 KG/CM²
(σ1 - σ3)max.
σ1 - σ3
Equivlent Pore Pressure
σ̄1 / σ̄3
STRESS (KG/CM²)
STRAIN (%)
3.0
2.0
1.0
0
-1.0
1.0
2.0
3.0
4.0
5.0

FIGURE 2.9

STATIC TRIAXIAL TEST
LOESS

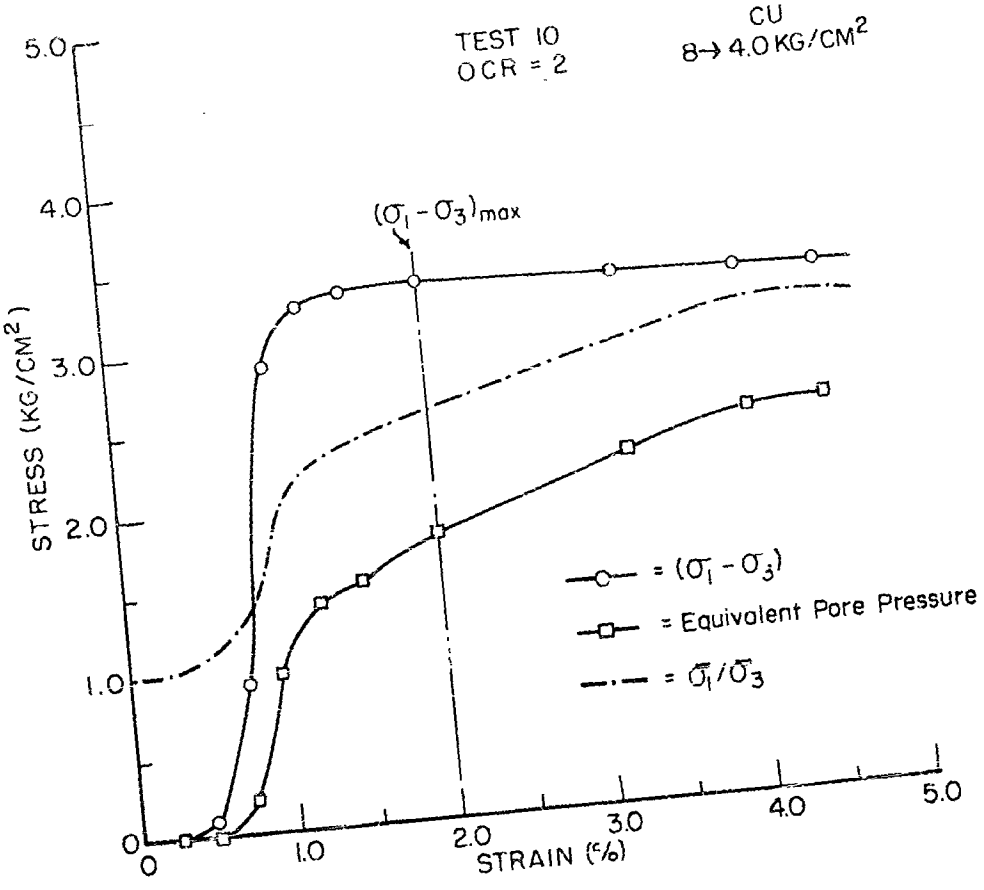

FIGURE 2.10

STATIC TRIAXIAL TEST
LOESS

TEST II CD
NC 3.0 KG/CM^2

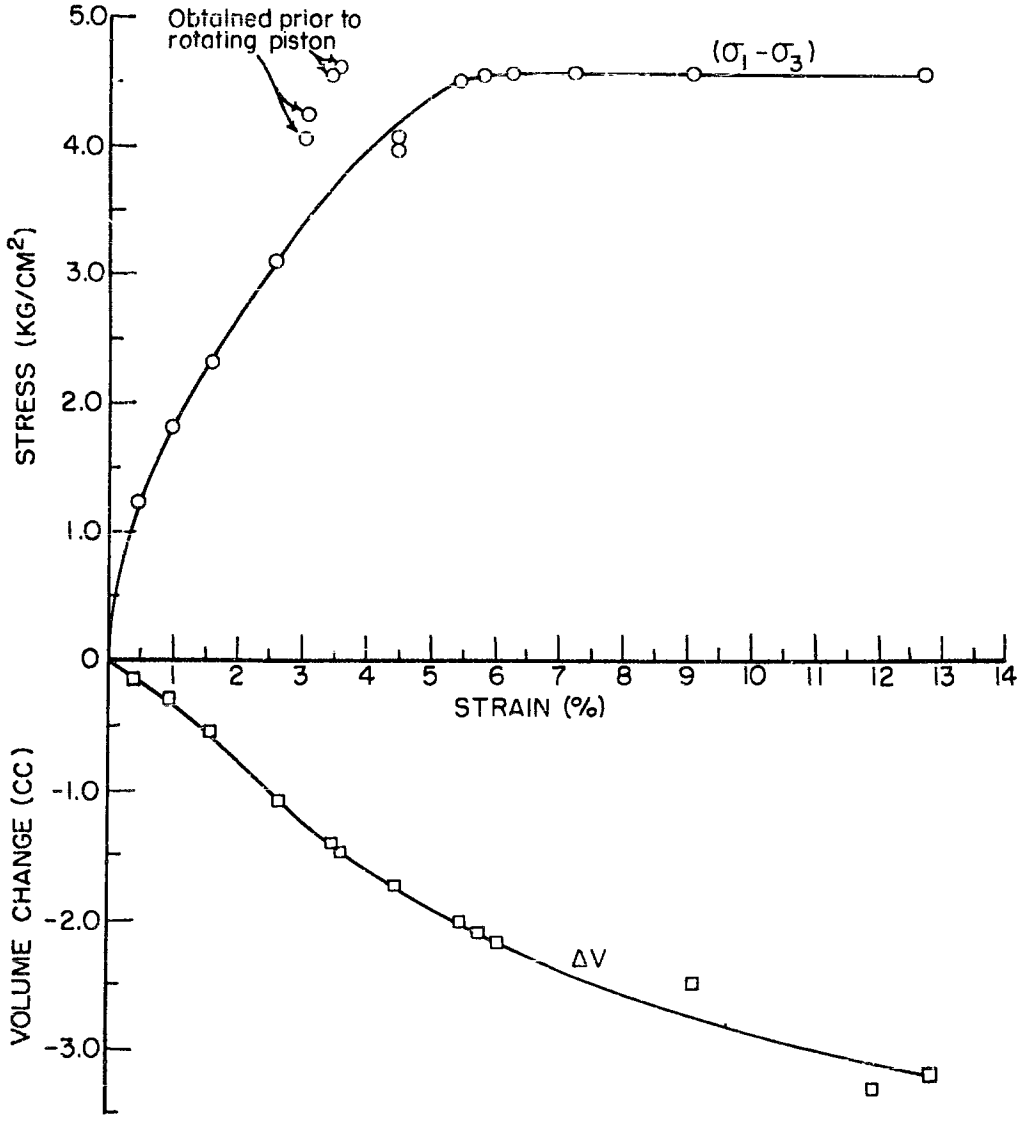

FIGURE 2.11

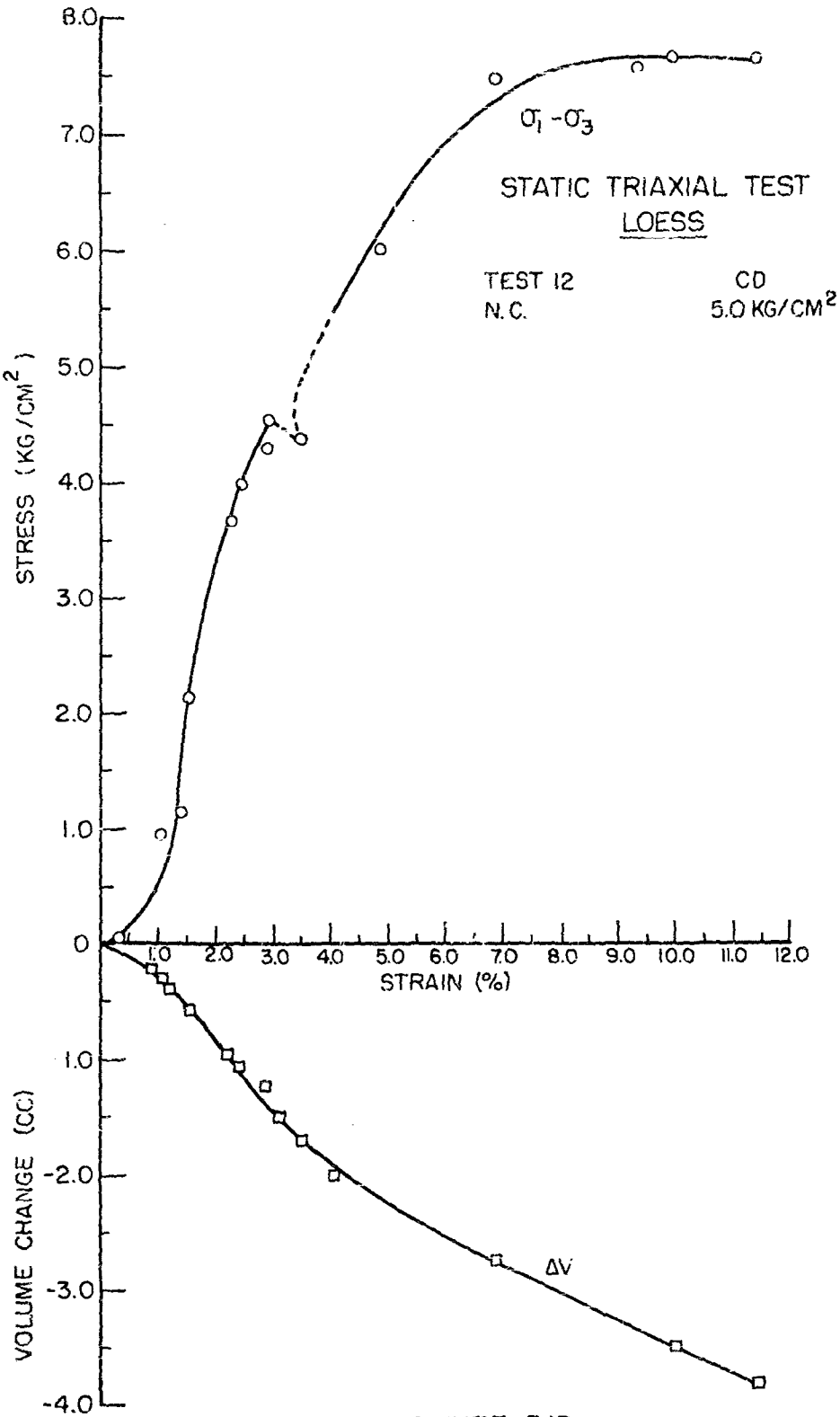
8.0
7.0
6.0
5.0
4.0
3.0
2.0
1.0
0
1.0
2.0
3.0
4.0
5.0
6.0
7.0
8.0
9.0
10.0
11.0
12.0
STRESS (KG/CM²)
STRAIN (%)
σ1 -σ3
STATIC TRIAXIAL TEST
LOESS
TEST 12
N.C.
CD
5.0 KG/CM²
VOLUME CHANGE (CC)
ΔV

FIGURE 2.12

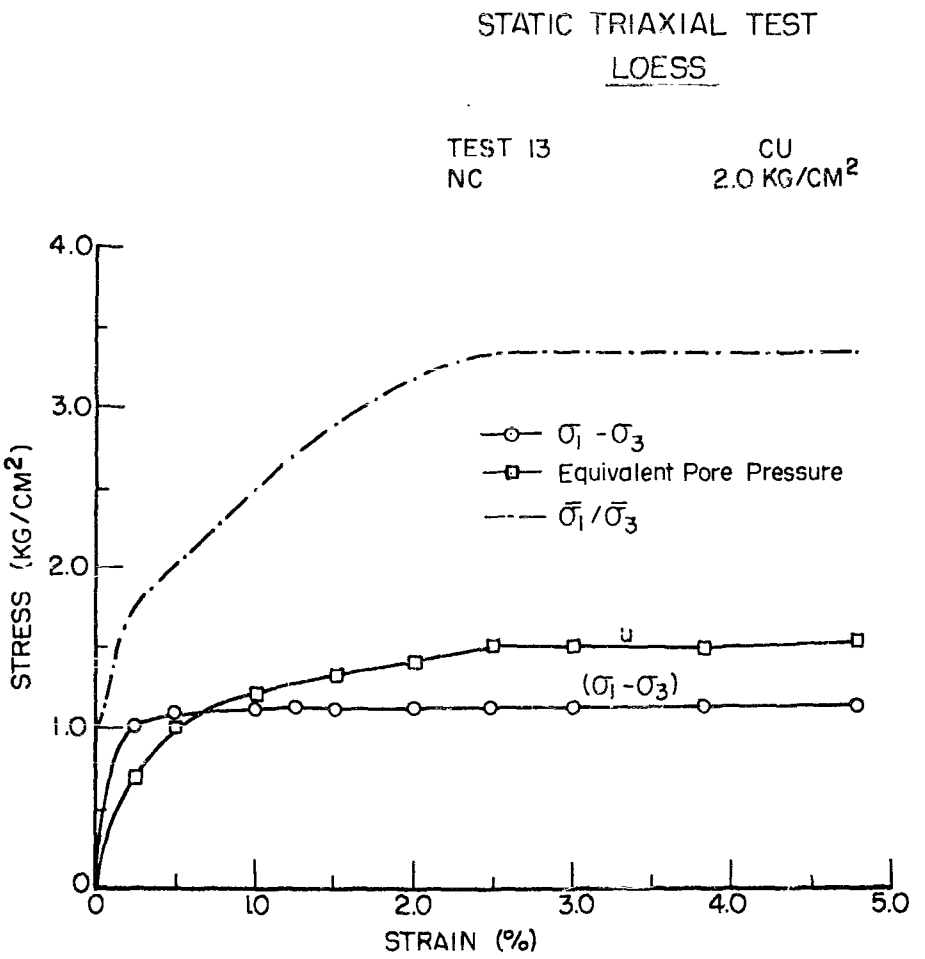
STATIC TRIAXIAL TEST
LOESS
TEST 13
NC
CU
2.0 KG/CM2
4.0
3.0
2.0
1.0
0
STRESS (KG/CM2)
σ1 -σ3
Equivalent Pore Pressure
σ̄1/σ̄3
u
(σ1-σ3)
0
1.0
2.0
3.0
4.0
5.0
STRAIN (%)

FIGURE 2.13

STATIC TRIAXIAL TEST
LOESS

TEST 14 CU
N. C. 4.00 KG/CM^2

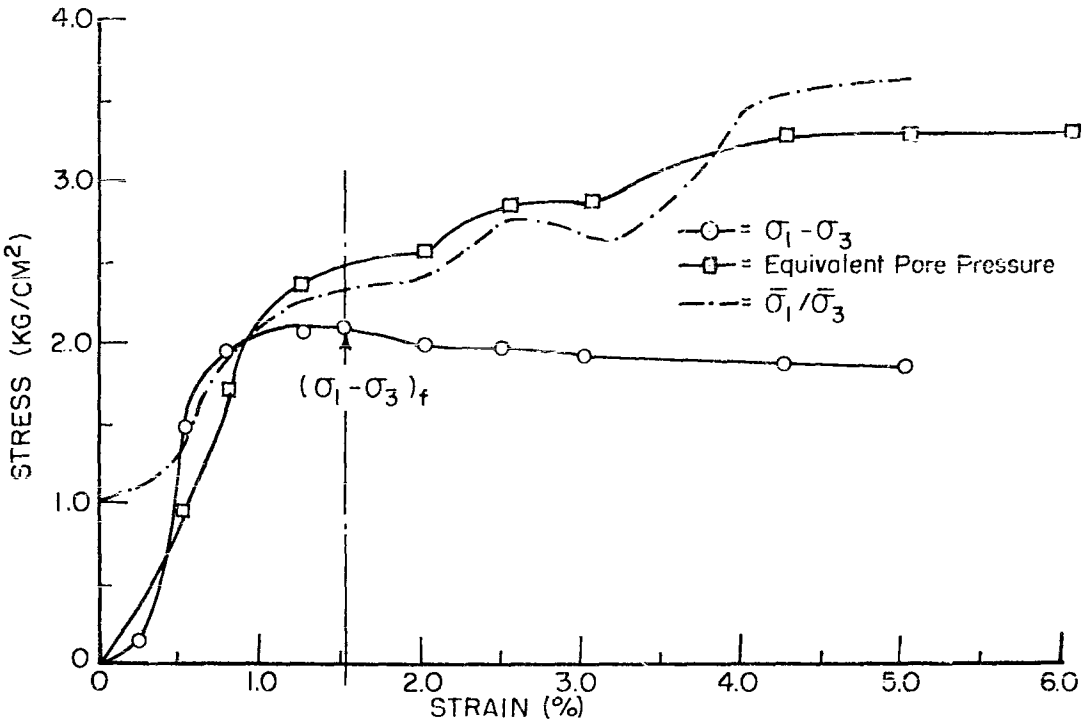

FIGURE 2.14

STATIC TRIAXIAL TEST

LOESS

TEST 15
N.C.

CU
8.00 KG/CM²

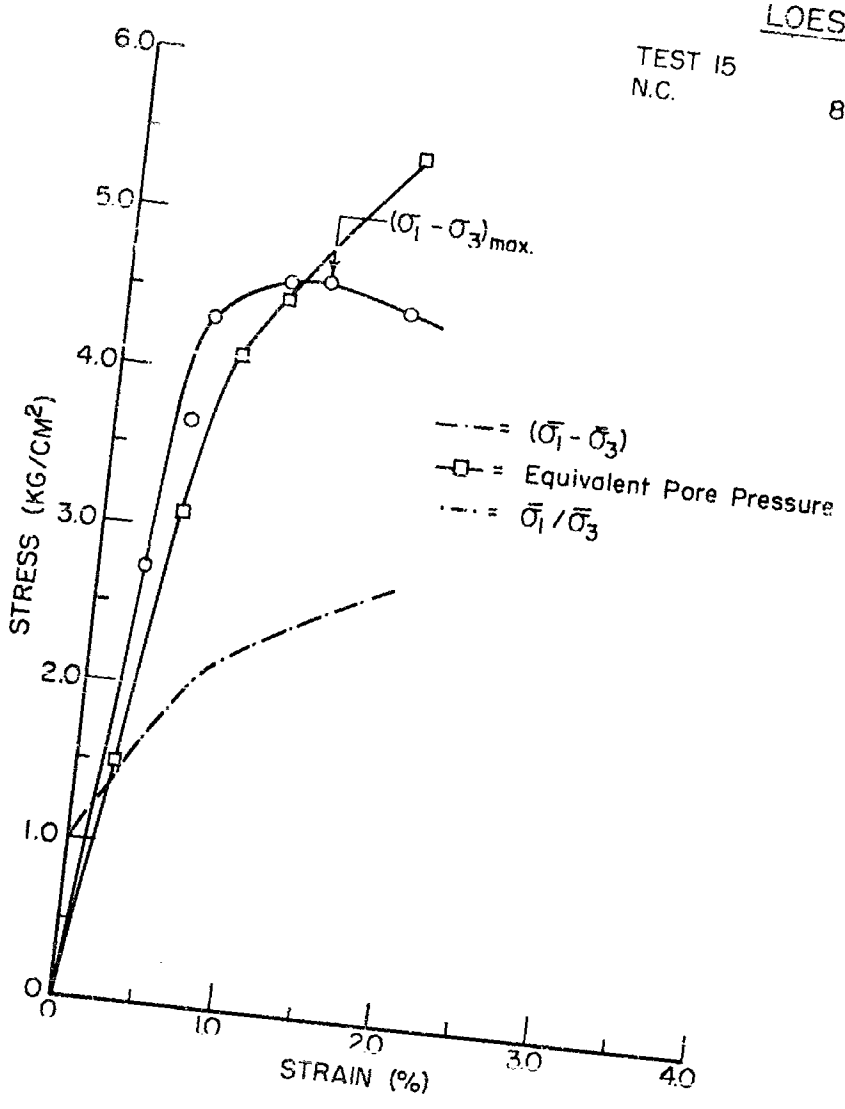

FIGURE 2.15

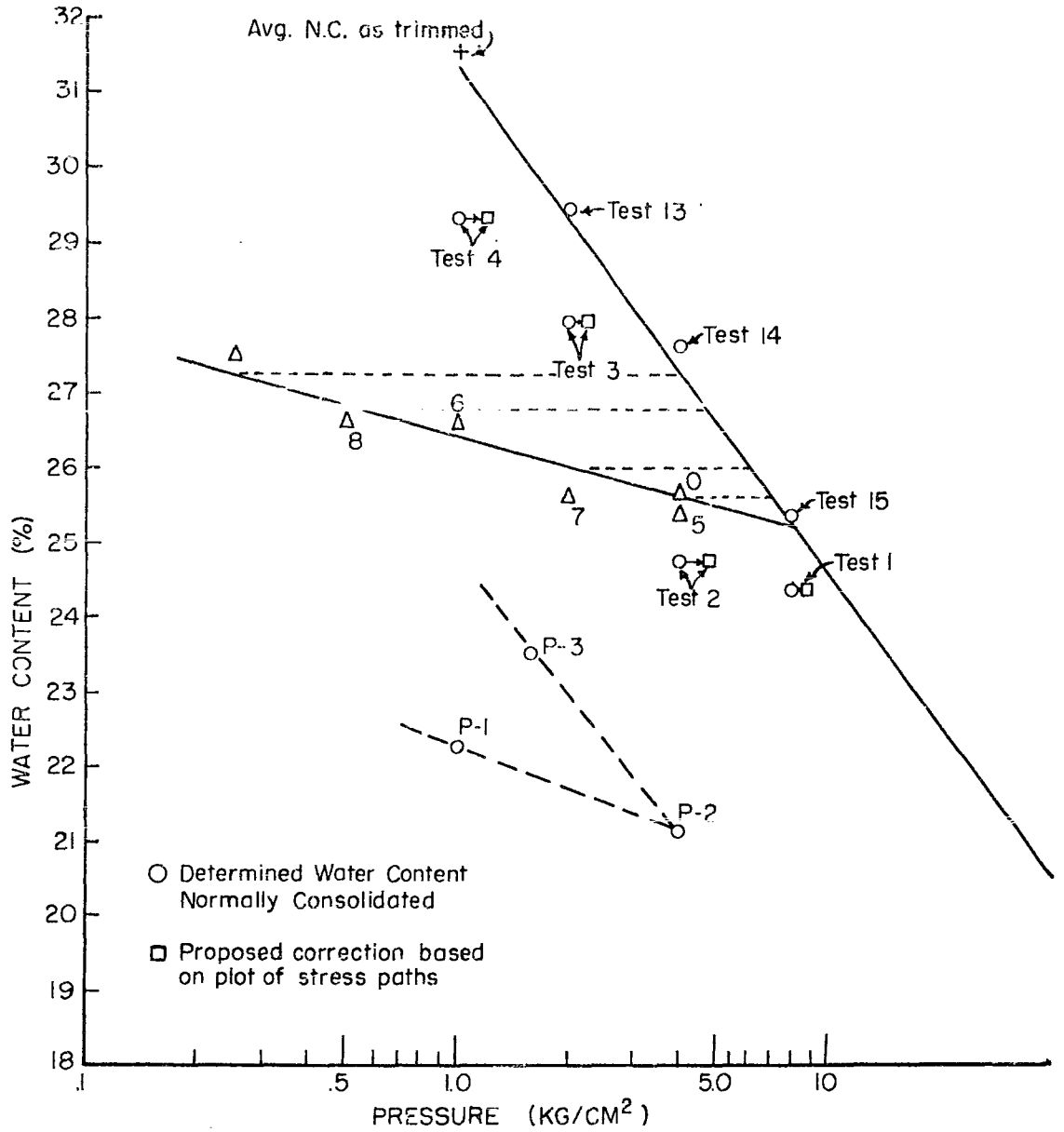

FIGURE 2.16 WATER CONTENT vs ISOTROPIC CONSOLIDATION PRESSURE - LOESS

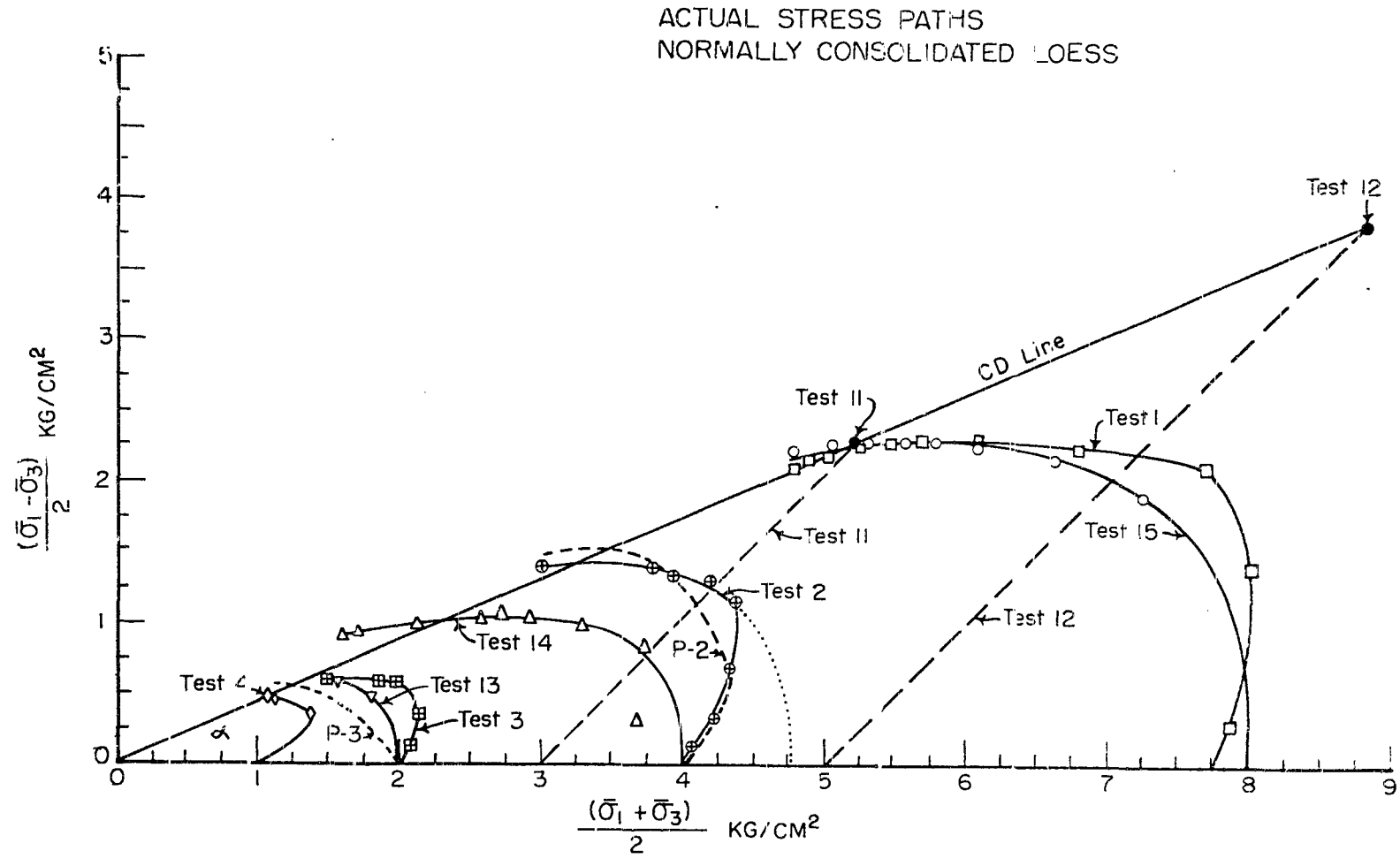
ACTUAL STRESS PATHS
NORMALLY CONSOLIDATED LOESS
Test 12
CD Line
Test 11
Test 1
Test 11
Test 15
Test 2
Test 12
Test 14
P-2
Test 4
Test 13
Test 3
P-3
0
1
2
3
4
5
6
7
8
9
$\frac{(\bar{\sigma}_1 - \bar{\sigma}_3)}{2}$ KG/CM²
$\frac{(\bar{\sigma}_1 + \bar{\sigma}_3)}{2}$ KG/CM²

FIGURE 2.17

NORMALIZING PLOT FOR NORMALLY CONSOLIDATED STRESS PATHS
& WATER CONTENT CONTOURS

LOESS

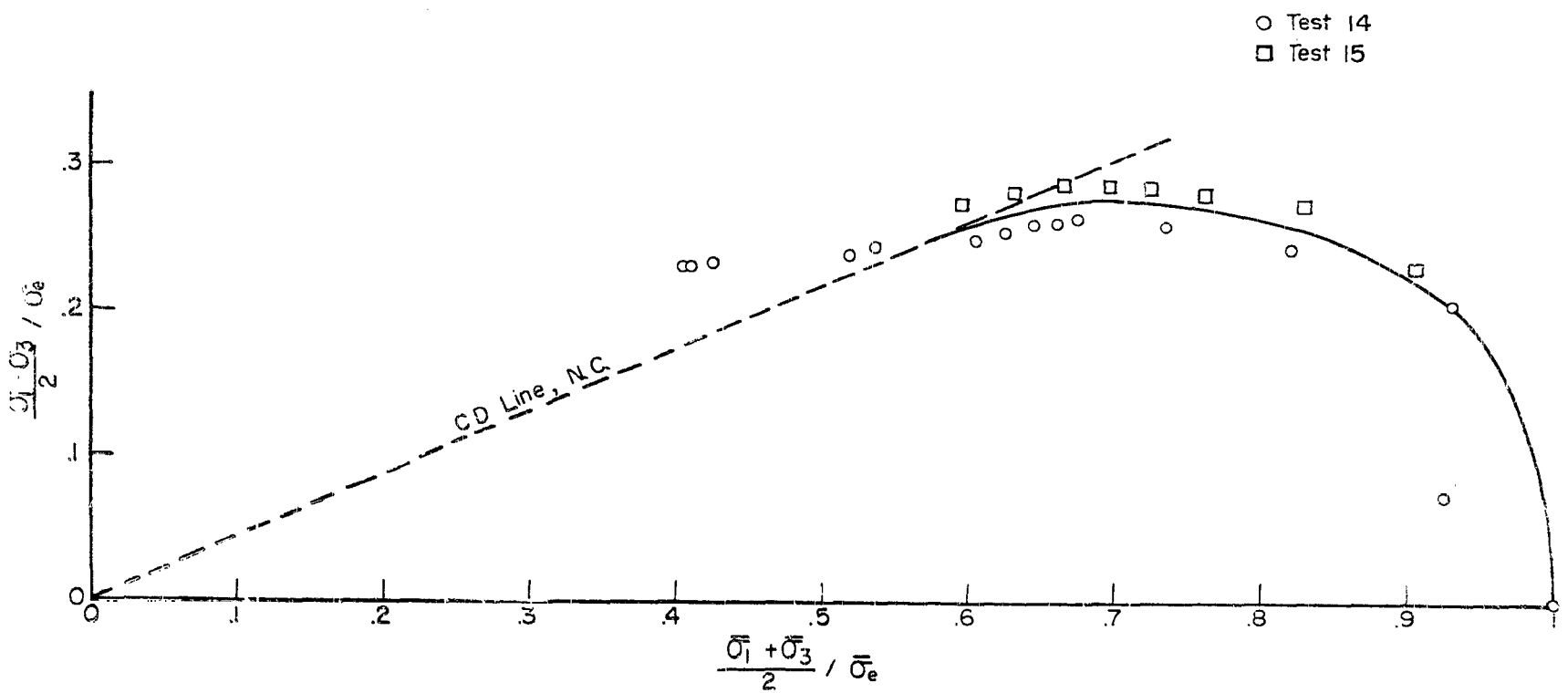

FIGURE 2.18

REMOLDED VICKSBURG LOESS
IDEALIZED NORMALLY CONSOLIDATED BEHAVIOR

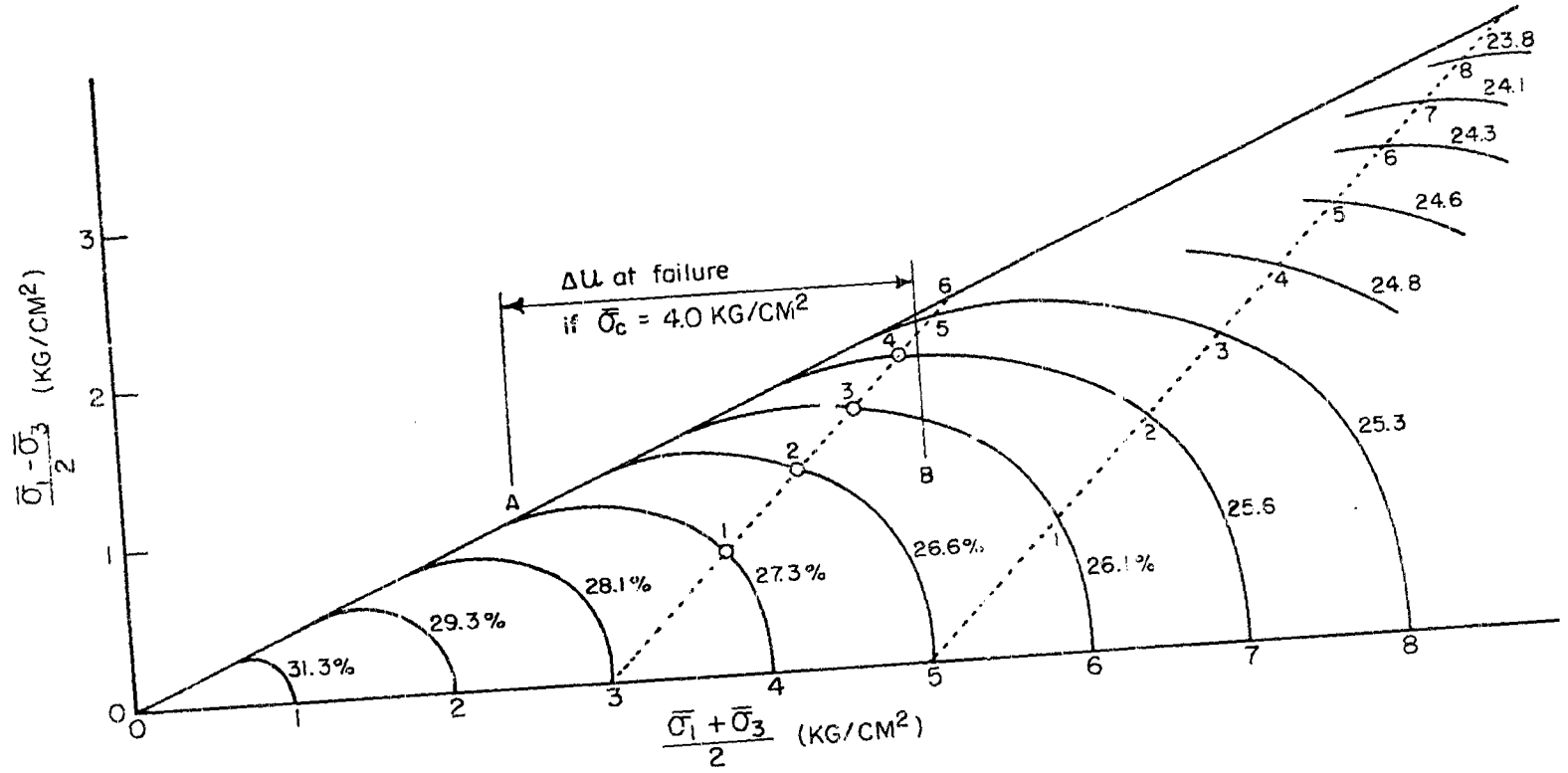

FIGURE 2.19

OVERCONSOLIDATED BEHAVIOR
LOESS
(MAX. σ_3 = 8.00 KG/CM^2)

Test	O.C.R.	ω_f	$\left(\frac{\sigma_1-\sigma_3}{2}\right)$ *Note: Failure
1	N.C.	24.4%	2.27
15	N.C.	25.4%	2.27
5	2	25.4%	2.18
10	2	25.7%	1.65
7	4	25.6%	1.50
6	8	26.6%	1.23
8	16	26.6%	1.15
9	32	27.5%	.92

*Note: Failure taken as O on stress paths

b = .32

α = Tan^{-1} .370

Sinϕ' = Tanα $\quad \phi' = 21° 30'$

$C = b\left(\frac{\text{Cos}\,\phi}{1-\text{Sin}^2\,\phi}\right) = 0.34$ KG/CM^2

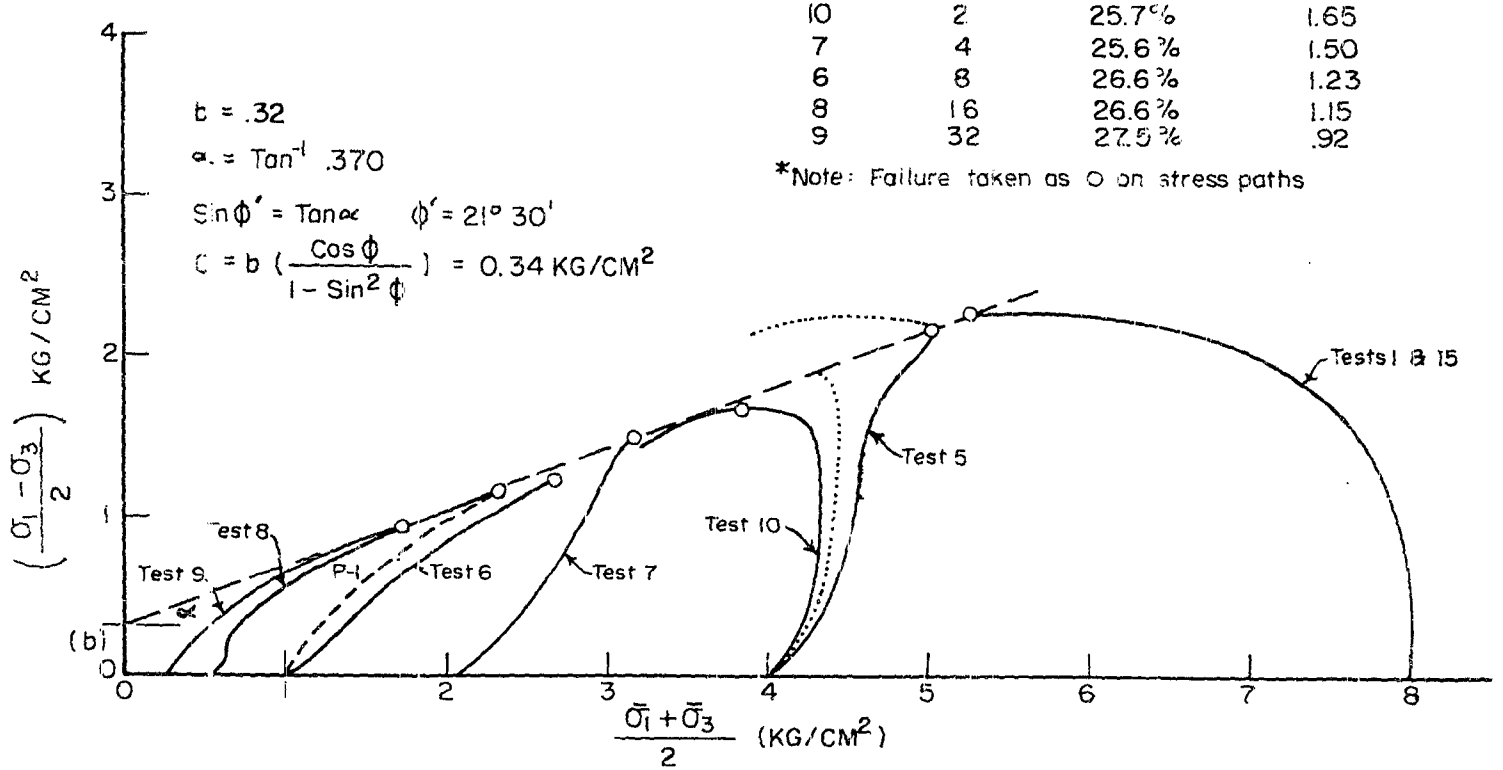

FIGURE 2.20

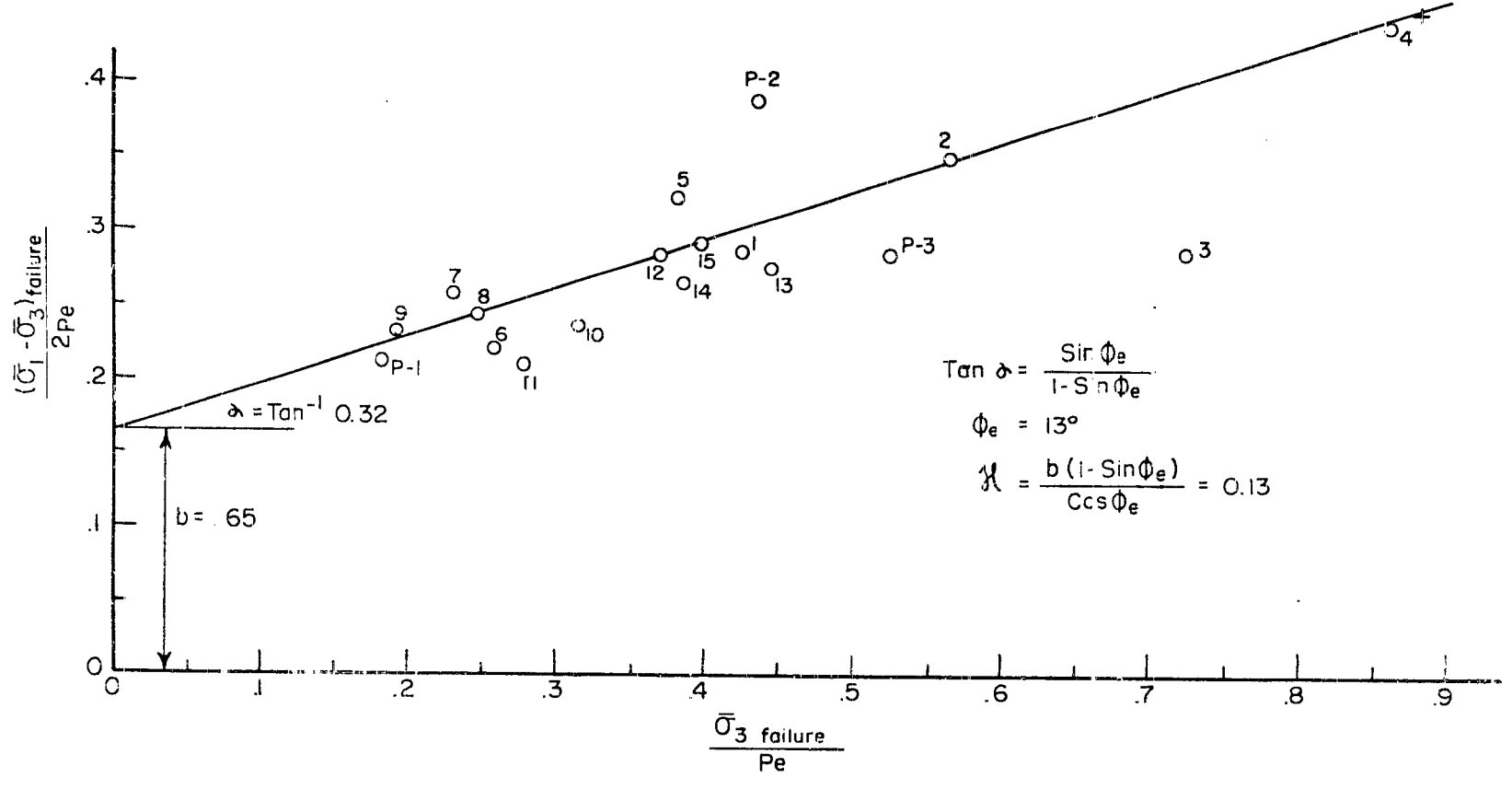

FIGURE 2.21 "HVORSLEV" PARAMETER PLOT-LOESS

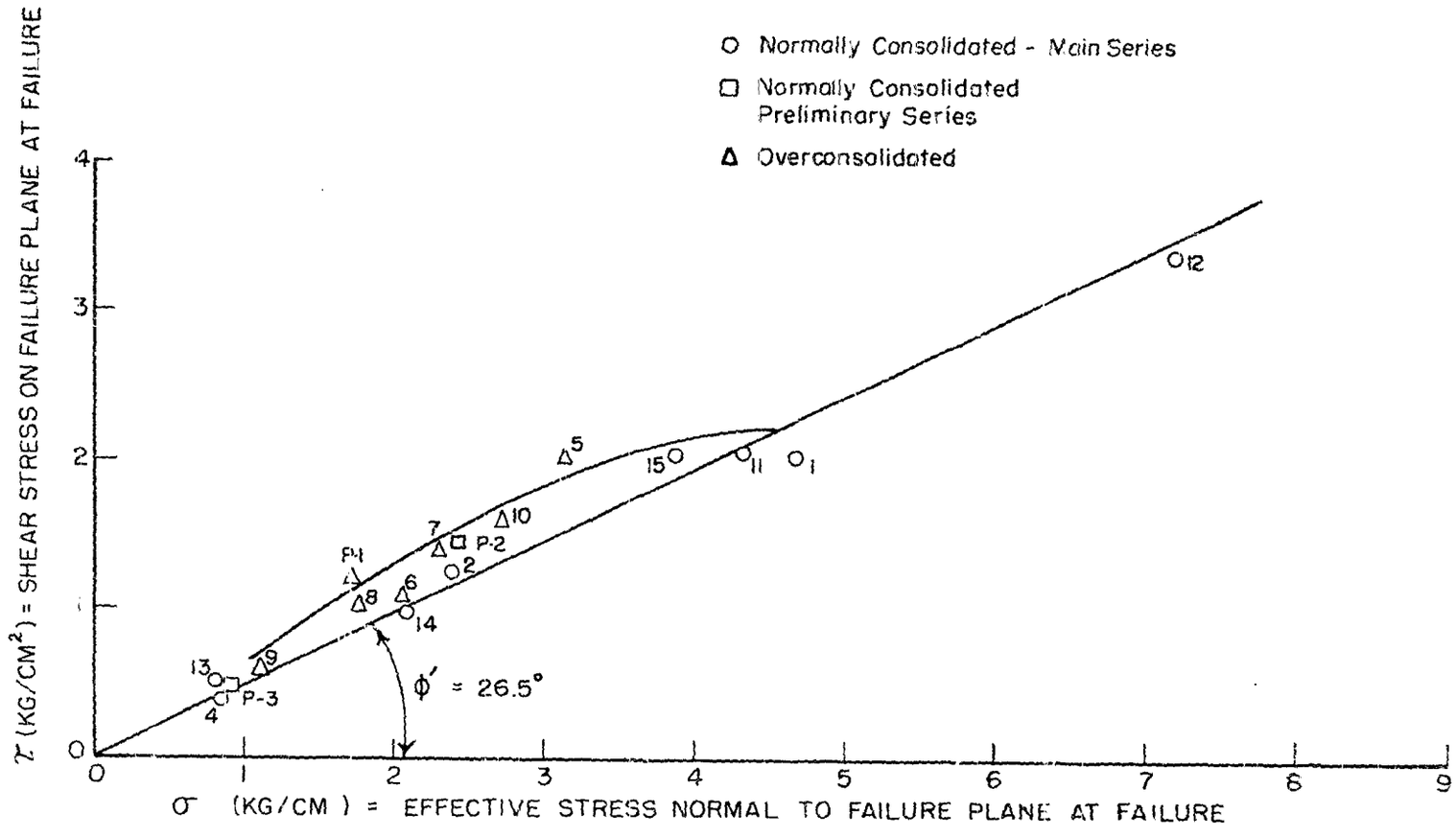

FIGURE 2.22 ENGINEERING EFFECTIVE STRESS vs SHEAR STRENGTH BEHAVIOR

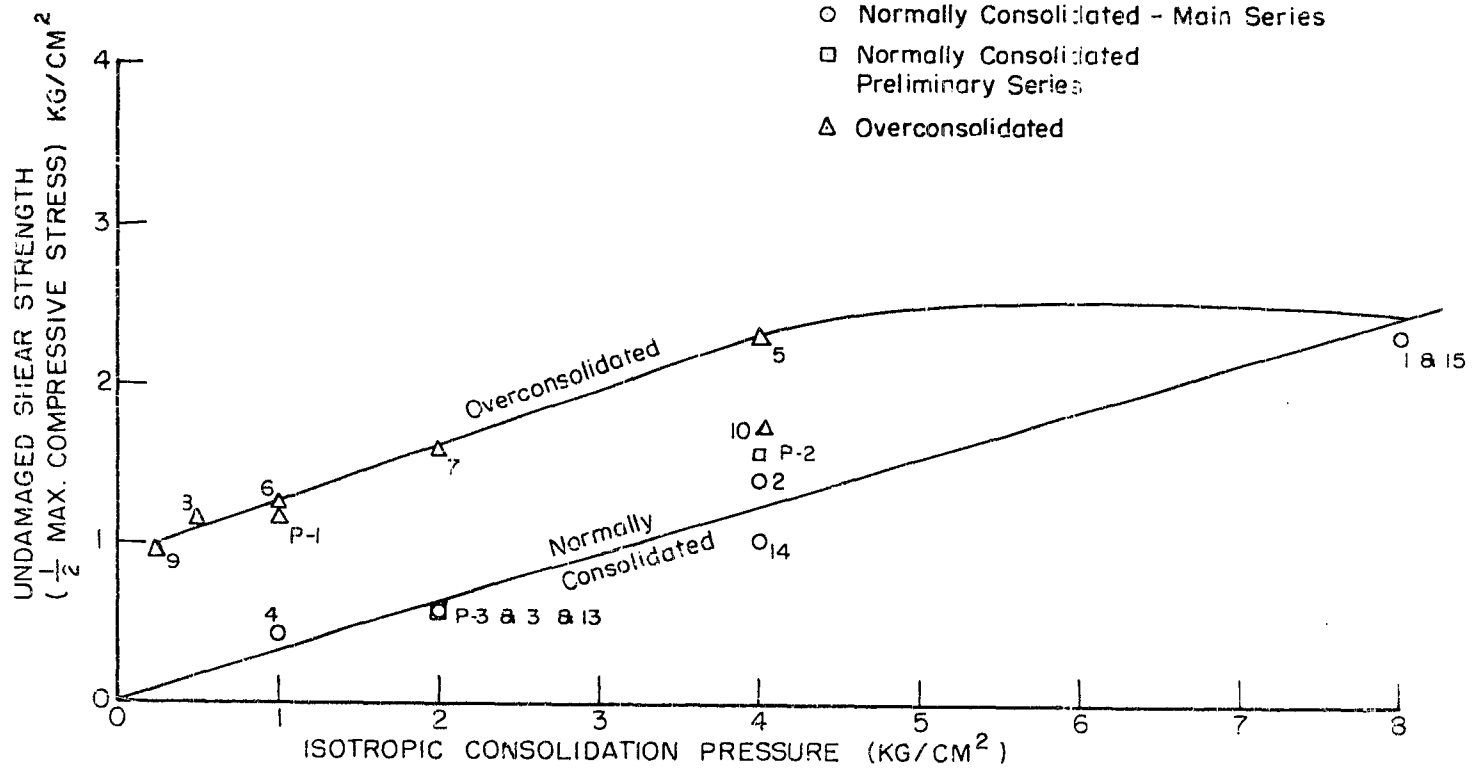

FIGURE 2.23 UNDRAINED SHEAR STRENGTH vs CONSOLIDATION PRESSURE

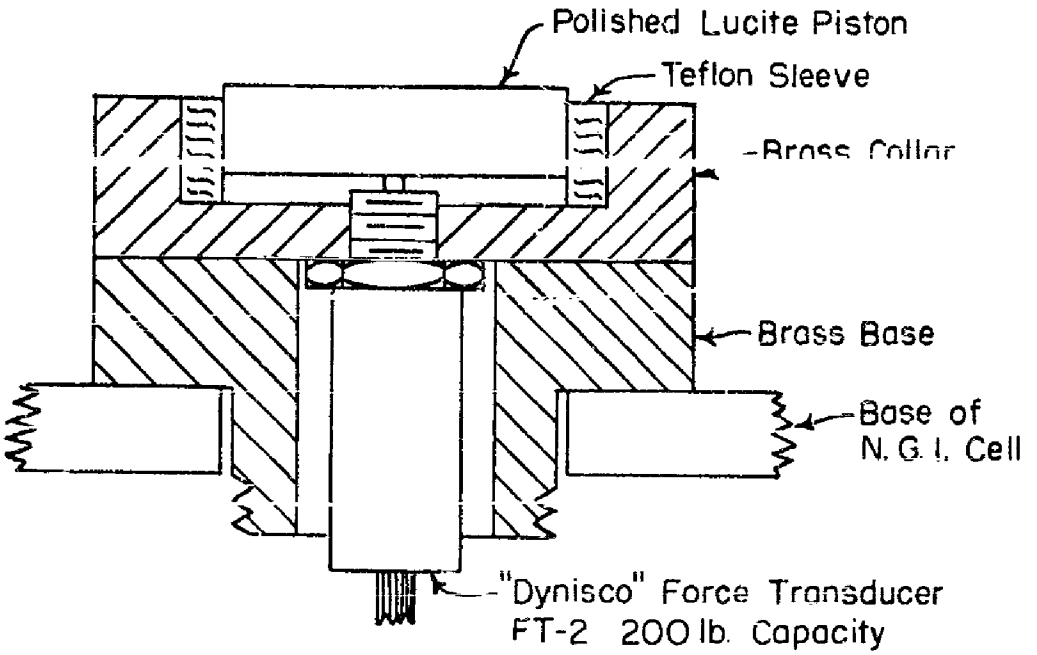

FIGURE 3.1 MODIFIED LOAD CELL

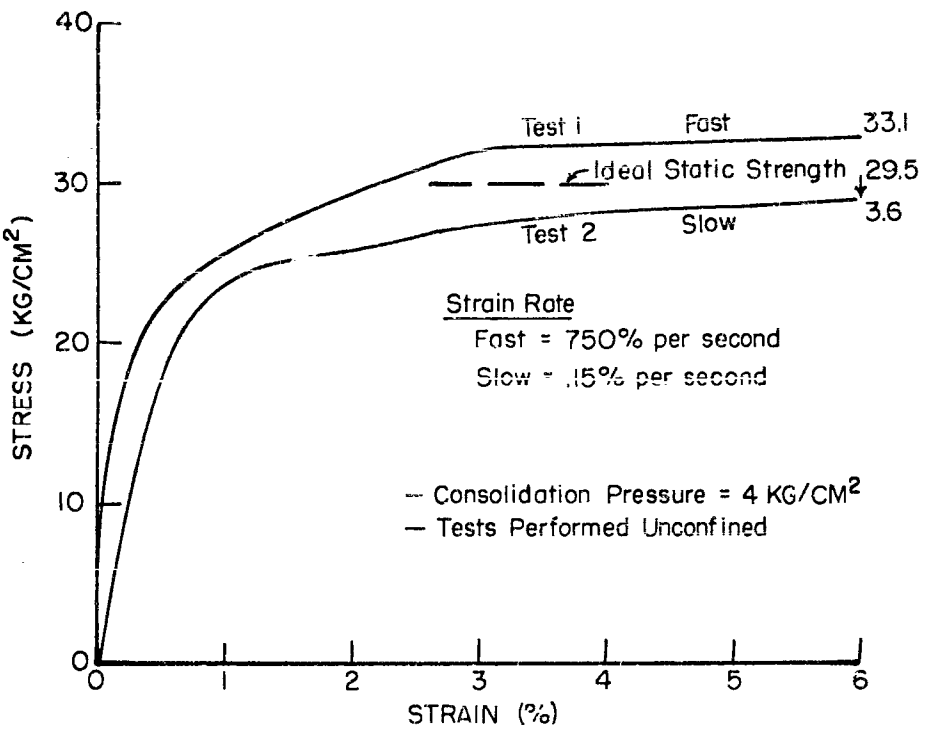

FIGURE 3.2 RAPID UNCONFINED COMPRESSION TESTS ON NORMALLY CONSOLIDATED LOESS

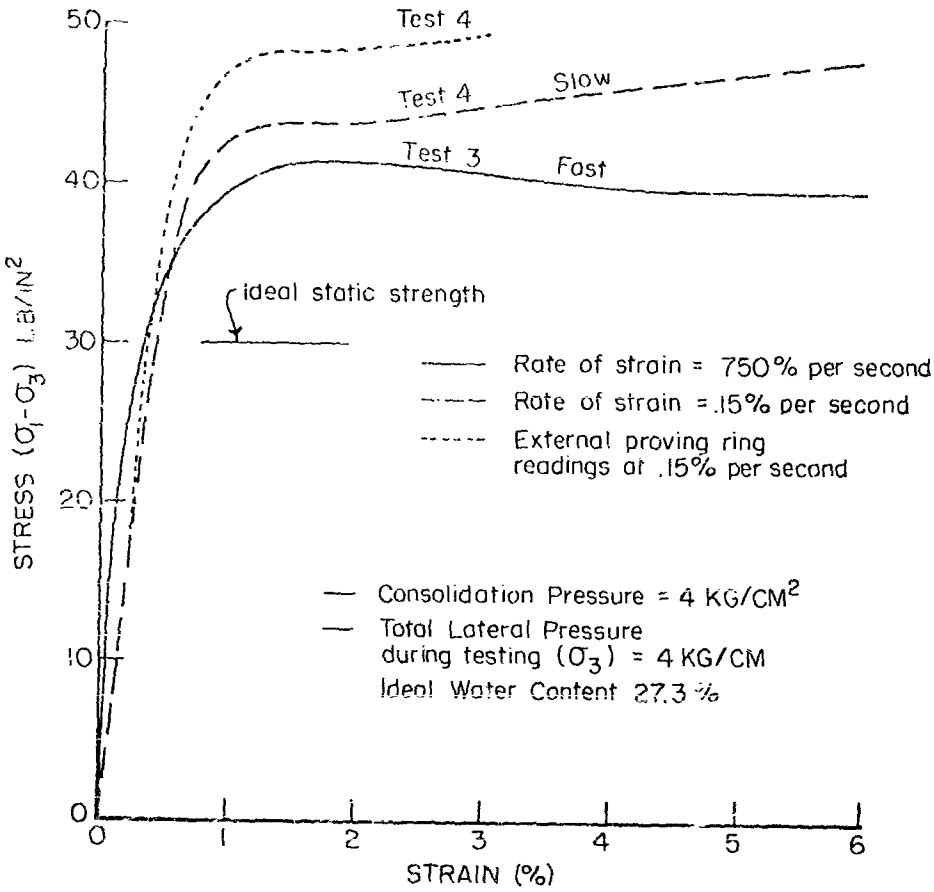

FIGURE 3.3 TRIAXIAL TESTS ON NORMALLY CONSOLIDATED LOESS

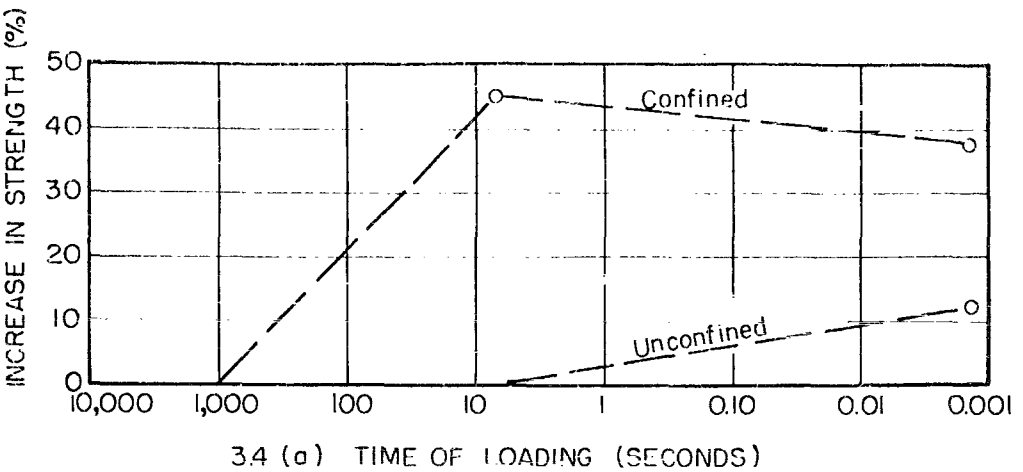

3.4 (a) TIME OF LOADING (SECONDS)

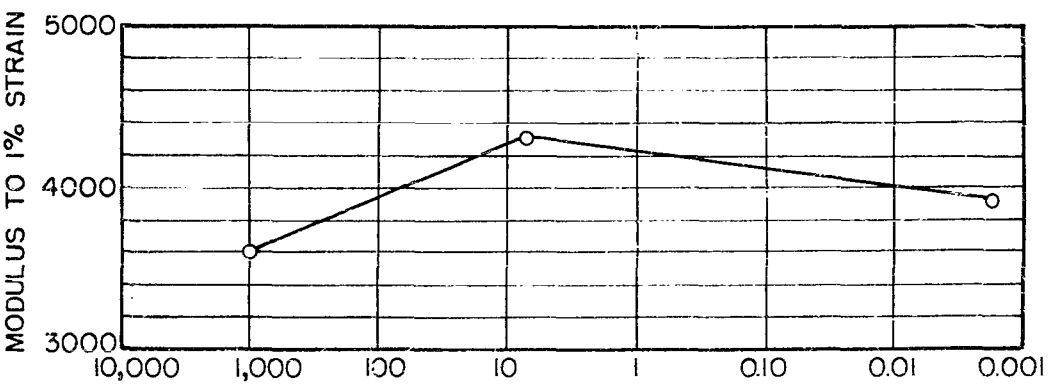

3.4 (b) TIME OF LOADING (SECONDS)

FIGURE 3.4 STRAIN RATE EFFECT - SATURATED LOESS

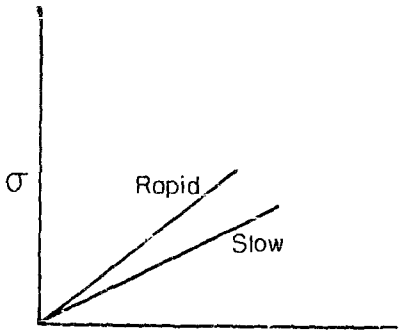

3.5(a) VISCOUS STRAIN RATE EFFECT

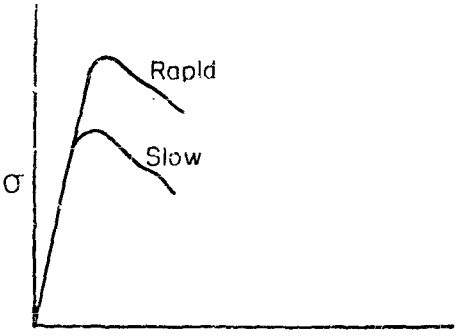

3.5(b) BRITTLE STRAIN RATE EFFECT

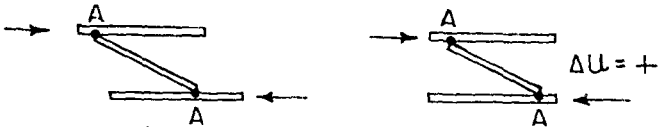

SLOW STRESS APPLICATION

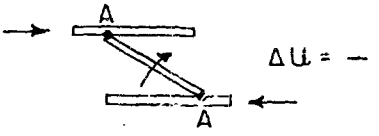

RAPID STRESS APPLICATION

3.5(c) MECHANISM CONTRIBUTING TO POSSIBLE CHANGE IN A AT A POINT

FIGURE 3.5 SKETCHES OF POSSIBLE STRAIN-RATE MECHANISMS

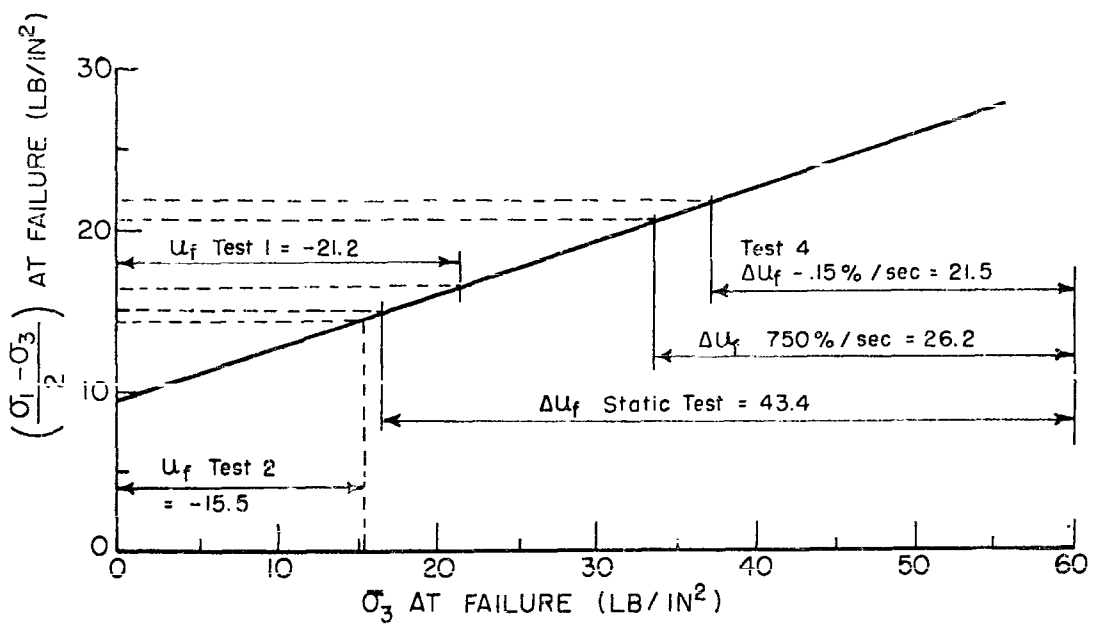

FIGURE 3.6 PLOT FOR WATER CONTENT AT FAILURE = 27.3%

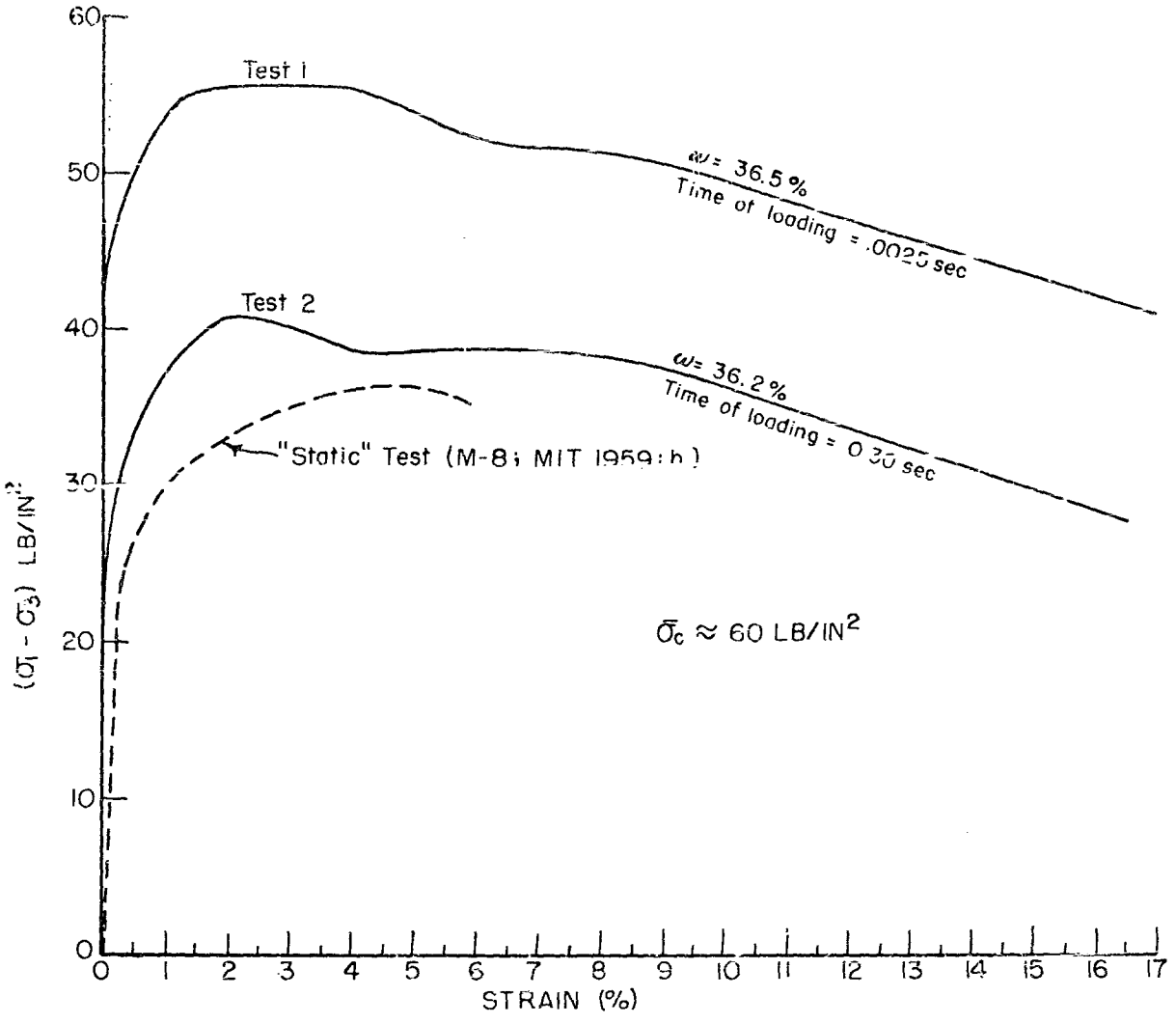

FIGURE 4.1 FAT CLAY - STRESS vs STRAIN BEHAVIOR - NORMALLY CONSOLIDATED

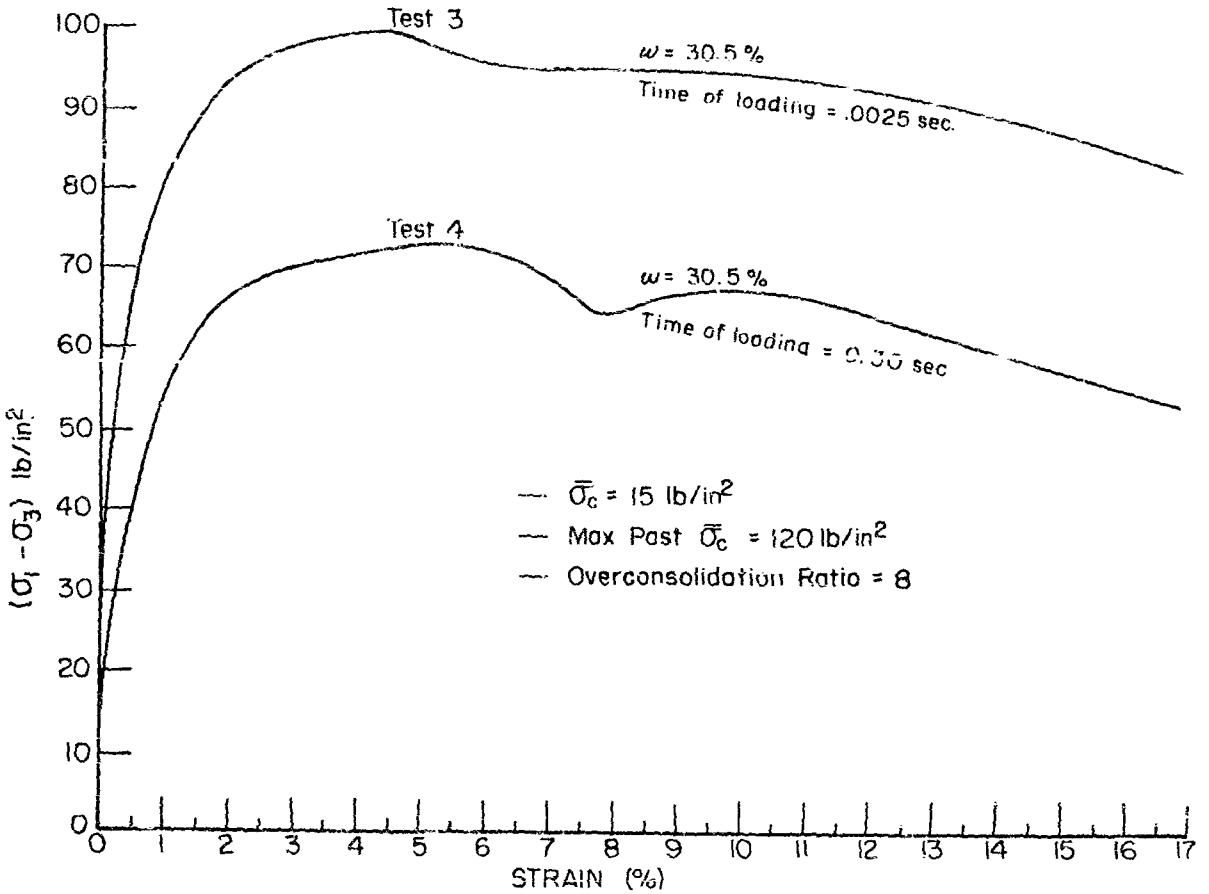

FIGURE 4.2 FAT CLAY - STRESS vs STRAIN BEHAVIOR - OVERCONSOLIDATED

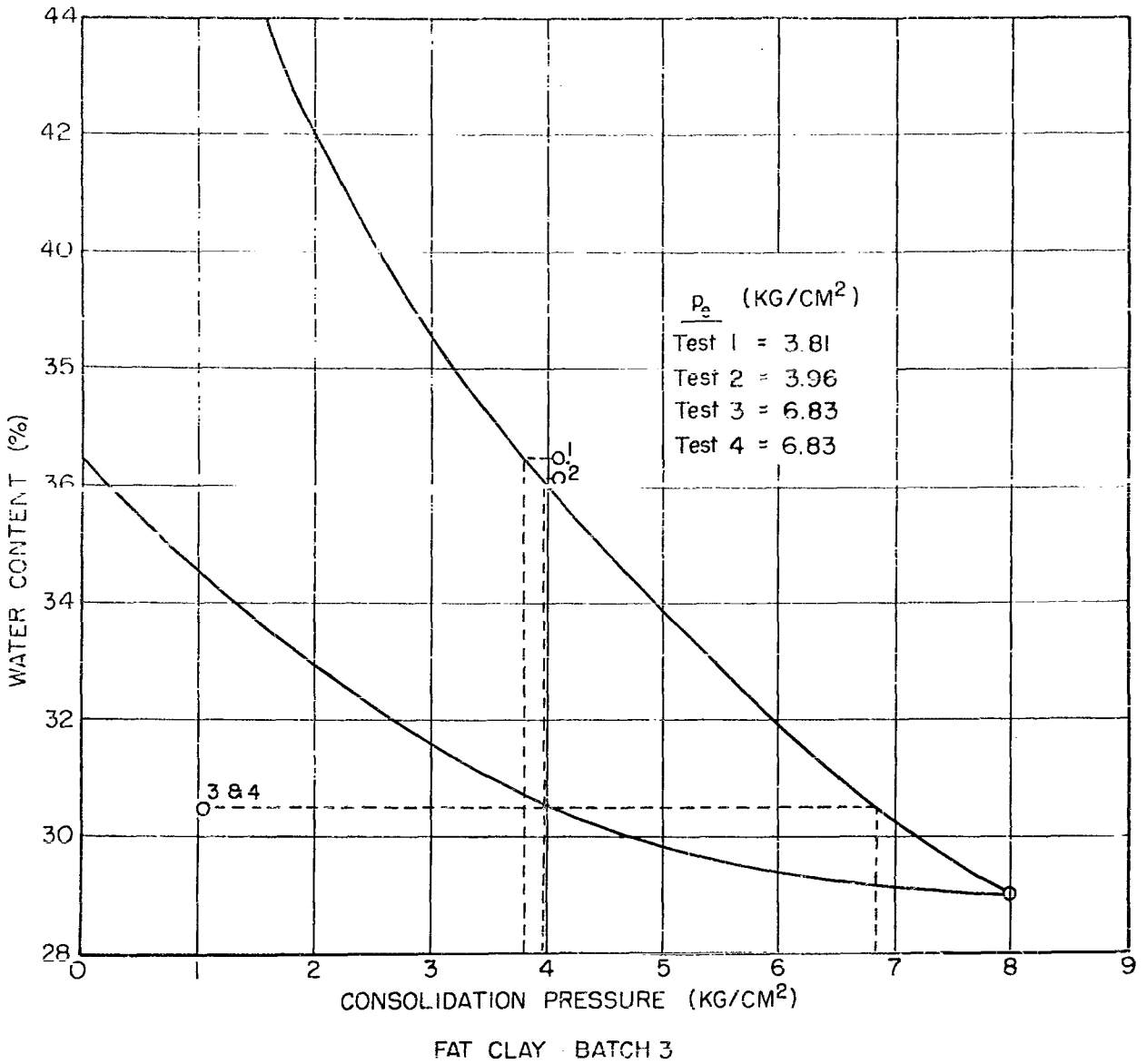

FIGURE 4.3 WATER CONTENT vs ISOTROPIC CONSOLIDATION PRESSURE

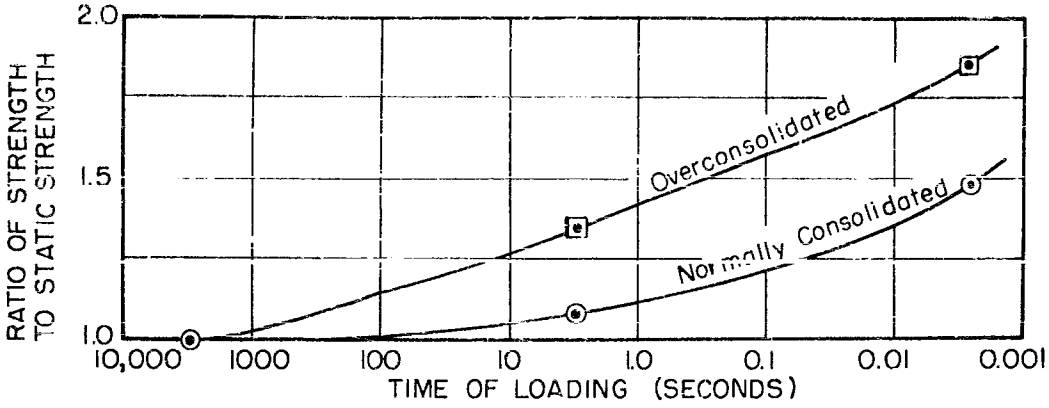

4.4(a) PLOT OF STRENGTH INCREASE vs TIME OF LOADING, FAT CLAY

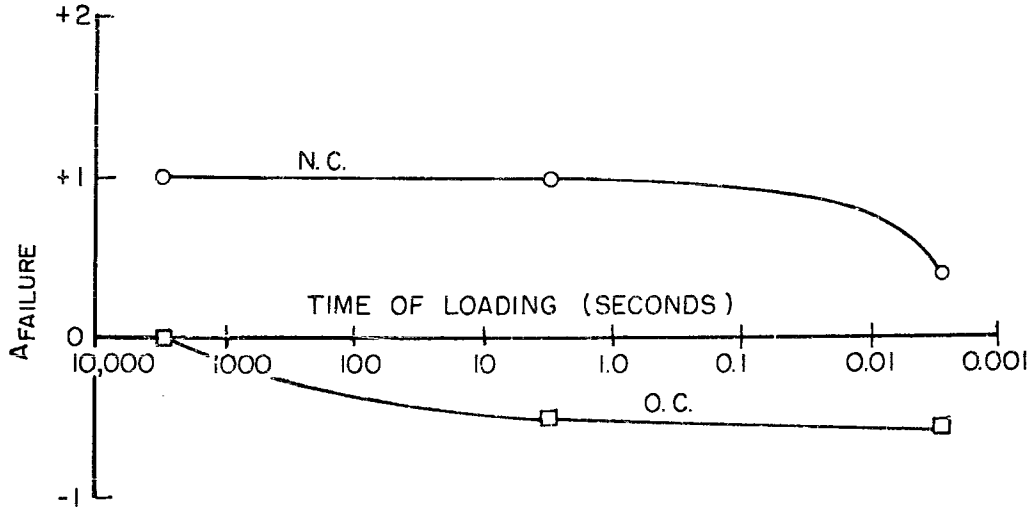

4.4 (b) PLOT OF DEDUCED PORE PRESSURE PARAMETER A vs TIME OF LOADING - FAT CLAY

FIGURE 4.4

LIST OF SYMBOLS

A	Corrected area at strain level
A_o	Area following consolidation
A, B	Pore pressure parameters relating pore pressure change to principal stress changes
c'	Cohesion in terms of effective stress
C_c	Compression index
c_e	True cohesion
C_r	Rebound index
G_s	Specific Gravity of solids
P_e	Equivalent consolidation pressure
w	Water content
$\mathcal{H}$	c_e/P_e
σ	Total stress
$\bar{\sigma}$	Effective stress
σ_1	Major principal stress
σ_2	Intermediate principal stress
σ_3	Minor principal stress
σ_{ff}	effective stress on failure plane at failure
Δ	Change
$\Delta\bar{\sigma}$	Incremental change in effective stress
τ	Shear stress
τ_{ff}	Shear stress on failure plane at failure, i.e., shear
u	Pore pressure

LIST OF SYMBOLS - Continued

ε	Unit strain
φ'	Angle of shearing resistance in terms of effective stress
φ_e	True angle of internal friction

BIBLIOGRAPHY

BISHOP, A. W., ALPAN, I. BLIGHT, G. E., AND DONALD, I. B., (1960),"Discussion and Closure to Session 2", Proc. ASCE Research Conference on Shear Strength of Cohesive Soils.

BISHOP, A. W. AND HENKEL, D. J. (1957), "The Measurement of Soil Properties in the Triaxial Test", E. Arnold, London.

HENKEL, D. J., "The Correlation Between Deformation, Pore Water Pressure and Strength Characteristics of Saturated Clays", Doctoral Thesis, Imperial College, University of London, London.

HVORSLEV, M. J. (1937), "Uber die Festigkeitsiegenschaften Gestorter Bindiger Boden," Danmarks Naturvidenskabelige Samfund, Kopenhagen.

MIT (1959a) "Dynamics No. 2 - Test Equipment for High Speed Triaxial Tests", Report to the Waterways Experiment Station; Publication 100 of MIT Soil Engineering Division.

MIT (1959b) "Dynamics No. 3 - First Interim Report on Soil Tests", Report to the Waterways Experiment Station; DASA - 1162; Publication 104 of MIT Soil Soil Engineering Division

PENMAN, A.D.M., (1953), "Shear Characteristics of a Saturated Silt, Measured in Triaxial Compression," Geotechnique.

SKEMPTON, A. W. (1954), "The Pore Pressure Coefficients A and B", Geotechnique, Vol. 4.

WHITMAN, R. V., RICHARDSON, A.M.JR., HEALY, K.A.(1961), "Time Lags in Pore Pressure Measurements, 5th Internat. Conf., Internat. Soc. of S. M. and Found. Eng., Paris.

Defense Threat Reduction Agency
45045 Aviation Drive
Dulles, VA 20166-7517

CPWC/TRC

May 6, 1999

MEMORANDUM FOR DEFENSE TECHNICAL INFORMATION CENTER
ATTN: OCQ/MR WILLIAM BUSH

SUBJECT: DOCUMENT REVIEW

The Defense Threat Reduction Agency's Security Office has reviewed and declassified or assigned a new distribution statement:

- AFSWP-1069, AD-341090, STATEMENT A — RD waiting for reply
- DASA-1151, AD-227900, STATEMENT A
- DASA-1355-1, AD-336443, STATEMENT A
- DASA-1298, AD-285252, STATEMENT A
- DASA-1290, AD-444208, STATEMENT A
- DASA-1271, AD-276892, STATEMENT A
- DASA-1279, AD-281597, STATEMENT A
- DASA-1237, AD-272653, STATEMENT A
- DASA-1246, AD-279670, STATEMENT A
- DASA-1245, AD-419911, STATEMENT A
- DASA-1242, AD-279671, STATEMENT A
- DASA-1256, AD-280809, STATEMENT A
- DASA-1221, AD-243886, STATEMENT A
- DASA-1390, AD-340311, STATEMENT A — FRD
- ~~DASA-1283, AD-717097, STATEMENT A~~ OK
- DASA-1285-5, AD-443589, STATEMENT A
- DASA-1714, AD-473132, STATEMENT A
- DASA-2214, AD-854912, STATEMENT A
- DASA-2627, AD-514934, STATEMENT A
- DASA-2651, AD-514615, STATEMENT A
- ~~DASA-2536, AD-876697, STATEMENT A~~
- DASA-2722T-V3, AD-518506, STATEMENT A
- DNA-3042F, AD-525631, STATEMENT A
- DNA-2821Z-1, AD-522555, STATEMENT A

If you have any questions, please call me at 703-325-1034.

Ardith Jarrett

ARDITH JARRETT
Chief, Technical Resource Center